LBL-33077
UC-414

Lawrence Berkeley Laboratory
UNIVERSITY OF CALIFORNIA

Presented at the NATO Advanced Study Institute "Particle Production in Highly Excited Matter," Il Ciocco, Lucca, Italy, July 12–25, 1992, and to be published in the Proceedings

From the Bevalac to RHIC: Recent Results and Future Perspectives

J.W. Harris

September 1992

REFERENCE COPY
Does Not
Circulate
Bldg. 50 Library.
LBL-33077
Copy 1

Prepared for the U.S. Department of Energy under Contract Number DE-AC03-76SF00098

DISCLAIMER

This document was prepared as an account of work sponsored by the United States Government. Neither the United States Government nor any agency thereof, nor The Regents of the University of California, nor any of their employees, makes any warranty, express or implied, or assumes any legal liability or responsibility for the accuracy, completeness, or usefulness of any information, apparatus, product, or process disclosed, or represents that its use would not infringe privately owned rights. Reference herein to any specific commercial product, process, or service by its trade name, trademark, manufacturer, or otherwise, does not necessarily constitute or imply its endorsement, recommendation, or favoring by the United States Government or any agency thereof, or The Regents of the University of California. The views and opinions of authors expressed herein do not necessarily state or reflect those of the United States Government or any agency thereof or The Regents of the University of California and shall not be used for advertising or product endorsement purposes.

Lawrence Berkeley Laboratory is an equal opportunity employer.

DISCLAIMER

This document was prepared as an account of work sponsored by the United States Government. While this document is believed to contain correct information, neither the United States Government nor any agency thereof, nor the Regents of the University of California, nor any of their employees, makes any warranty, express or implied, or assumes any legal responsibility for the accuracy, completeness, or usefulness of any information, apparatus, product, or process disclosed, or represents that its use would not infringe privately owned rights. Reference herein to any specific commercial product, process, or service by its trade name, trademark, manufacturer, or otherwise, does not necessarily constitute or imply its endorsement, recommendation, or favoring by the United States Government or any agency thereof, or the Regents of the University of California. The views and opinions of authors expressed herein do not necessarily state or reflect those of the United States Government or any agency thereof or the Regents of the University of California.

LBL-33077
UC-414

Presented at the NATO Advanced Study Institute
"Particle Production in Highly Excited Matter,"
Il Ciocco, Lucca, Italy, July 12-25, 1992
and to be published in the Proceedings

From the Bevalac to RHIC: Recent Results and Future Perspectives

John W. Harris
Lawrence Berkeley Laboratory
University of California, Berkeley, CA 94720

September 1992

This work was supported by the Director, Office of Energy Research, Division of Nuclear Physics of the Office of High Energy and Nuclear Physics of the U.S. Department of Energy under Contract DE-AC03-76SF00098

FROM THE BEVALAC TO RHIC: RECENT RESULTS AND FUTURE PERSPECTIVES

John W. Harris
Nuclear Science Division, Lawrence Berkeley Laboratory
University of California, Berkeley CA 94720

ABSTRACT

There has been considerable theoretical progress and experimental development in the study of relativistic nucleus-nucleus collisions towards understanding the equation of state of nuclear, hadronic and partonic matter. At high energies, research has concentrated on the search for the quark-gluon plasma (QGP) and possible chiral symmetry restoration. In these lectures I comment on similarities and trends observed in **recent results** over a wide range of incident energies and attempt to provide a common framework where possible. I also point out **future perspectives** in the search for the QGP at the Relativistic Heavy Ion Collider (RHIC), and in particular focus on one experiment to be undertaken.

INTRODUCTION

Preface

In the collisions of nuclei at extremely high energies the baryon and energy densities are expected to reach critical values where the quark constituents of the incident nucleons, bound in nuclei, form an extended volume of freely interacting quarks, antiquarks and gluons known as the quark-gluon plasma (QGP). After formation the system is expected to evolve dynamically from a pure plasma or mixed phase (of plasma and hadronic matter) through expansion, cooling, hadronization and freeze-out. To be able to establish that such a new, transient state of matter has been formed it will be necessary to identify and study QGP signatures and the space-time evolution of the collision process. This requires an understanding of the microscopic structure of hadronic interactions, at the level of quarks and gluons, at high temperatures and high densities.

The first of these two lectures will concentrate on **recent results** in the search for the QGP with an emphasis on similarities and trends in the data which have been obtained for a variety of systems at the available energies. This will not be an in-depth review of developments in the field, but rather comments on topics and trends of interest. The reader should consult other, specialized lectures in this summer school for more detail on specific topics. The second lecture will focus on **future perspectives** in the search for the QGP at the Relativistic Heavy Ion Collider (RHIC)[1] and will concentrate on one of the experiments to be undertaken there.

Pioneering Theoretical Developments

The primary motivation for studying nucleus-nucleus collisions at relativistic energies is to understand the equation of state of nuclear, hadronic and partonic matter at high temperatures and densities. Early speculations of possible exotic states of matter focused on the astrophysical implications of abnormal states of dense nuclear matter.[2,3,4]

Subsequent field theoretical calculations, assuming chiral symmetry in the σ model, resulted in predictions of abnormal nuclear states and excitation of the vacuum.[5] This generated an interest in transforming the state of the vacuum by using relativistic nucleus-nucleus collisions.[6,7] Shortly thereafter, a deconfinement phase transition to quark matter or a quark-gluon plasma[8,9,10] was predicted. At the same time there were also predictions of phase transitions resulting from pion condensation in nuclear matter[11] with possible formation of the condensate in relativistic nucleus-nucleus collisions.[12] Many theoretical developments have evolved the field to its present state of understanding.[13] Presently, perturbative quantum chromodynamics (QCD) is being used to predict observables in experiments at ultrarelativistic energies and to calculate the properties of the high parton density matter, sometimes referred to as QCD matter, resulting from parton cascades in these collisions.[14]

Evolution of Relativistic Heavy Ion Accelerators

In 1974 the Bevalac at Lawrence Berkeley Laboratory began accelerating nuclear beams of masses $A \leq 38$ at energies up to $E_{lab} = 2.1$ GeV per nucleon. Since then many experiments have taken place at the Bevalac and other high energy nuclear beam accelerators. These include the Dubna Synchophasotron ($A \leq 20$, $E_{lab} \leq 4.2$ GeV/n), the CERN Super Proton Synchrotron (SPS) ($A \leq 32$, $E_{lab} \leq 200$ GeV/n), the Brookhaven Alternating Gradient Synchrotron (AGS) ($A \leq 28$, $E_{lab} \leq 13.6$ GeV/n) and the GSI SIS accelerator (SIS) ($A \leq 238$, $E_{lab} \leq 1.0$ GeV/n). In addition, the Dubna Nuclotron ($A \leq 238$, $E_{lab} \leq 6$ GeV/n) and the Brookhaven Relativistic Heavy Ion Collider (RHIC) ($A \leq 238$, $E_{lab} \leq 200$ GeV/n per colliding beam) are under construction and there are plans for nuclear beams in the Large Hadron Collider (LHC) ($A \leq 238$, $E_{lab} \leq 3.8$ TeV/n per colliding beam) to be built at CERN. These accelerators can be divided primarily into two categories: 1) high energy proton accelerators "rejuvenated" for acceleration of nuclear beams (Bevalac, Synchophasotron, SPS and AGS) and 2) a new generation of dedicated high energy nuclear beam accelerators (SIS, Nuclotron and RHIC). The LHC with nuclear beams is in a separate category, namely a high energy physics machine to be designed and built from the outset with a heavy nuclear beam capability.

There are surprising similarities in the evolution of the accelerators, experiments and physics results. For purely technical reasons related to ion "sourcery" and available vacuum and injection techniques, the acceleration of heavy nuclear beams at the "rejuvenated" accelerators (Bevalac, AGS and SPS)[15] has proceeded in two steps. Initially, light nuclear beams ($A < 40$) have been accelerated followed several years later by an upgrade which enables the acceleration of heavier beams up to $A \sim 238$. On the other hand, the capability of accelerating the heaviest nuclear beams has been incorporated into the design of the dedicated nuclear beam accelerators.

Evolution of Experiments

The experiments at the existing relativistic nuclear beam facilities have typically undertaken initial measurements of inclusive observables such as transverse momentum and rapidity distributions of particles. The intranuclear cascade[16] calculations were able to reproduce the inclusive data in light nuclear systems ($A < 40$) from the Bevalac and likewise the Lund/FRITIOF[17] model reproduced the initial AGS and SPS data. This is simply due to the models' incorporation of the correct reaction processes and kinematics for the respective collisions coupled with the absence of any large signal of new phenomena in the measured inclusive data. Subsequent models with sometimes diametrically opposite assumptions about the primary reaction mechanisms have also been able to reproduce the inclusive measurements.

Multiparticle and semi-exclusive experiments are typically more complicated than inclusive experiments, requiring more time to construct and assemble, for analysis of data and to understand the efficiencies of the detector. Consequently, a significantly longer time for extraction of physics results is necessary for these measurements. However, semi-exclusive and triple-differential measurements have been able to distinguish between models which were previously able to reproduce the measured inclusive results. Likewise, second generation experiments which allow expanded coverage in some combination of statistics, particle type and phase space have made available a more detailed view of the reaction mechanism and often distinguish between theoretical models. In the case of the Bevalac, a combination of second generation detectors and multiparticle observables coupled with the availability of the heavier beams ($40 \leq A \leq 238$) made it possible to unequivocally observe new phenomena, collective nuclear flow.[18,19] A similar development is the goal of the new experiments utilizing the heavier beams at the AGS and SPS.

PARTICLE SPECTRA

Motivation

In the search for a phase transition from normal nuclear or hadronic matter to a quark-gluon plasma, the transverse momentum spectra of particles have been of particular interest. Although the detailed shape of the spectra can be modified by many factors, the average behavior may reflect one characteristic of a phase transition. In an analogy between the water-vapor phase transition and the nuclear matter-QGP phase transition, each system starts out in the lower temperature state. Upon heating, the system reaches a transition temperature at which it remains in a mixed phase for some period of time until all the matter is transformed into the higher temperature state. This results in a characteristic curve of the temperature as a function the entropy density. This was elucidated by Van Hove[20] and is depicted in Fig. 1a. Van Hove proposed that in high energy collisions the mean transverse momentum is a measure of the temperature of the system and that the multiplicity or energy density reflects the entropy density. The curve is characterized by a rise upon initial heating, a plateau during the mixed phase and a second

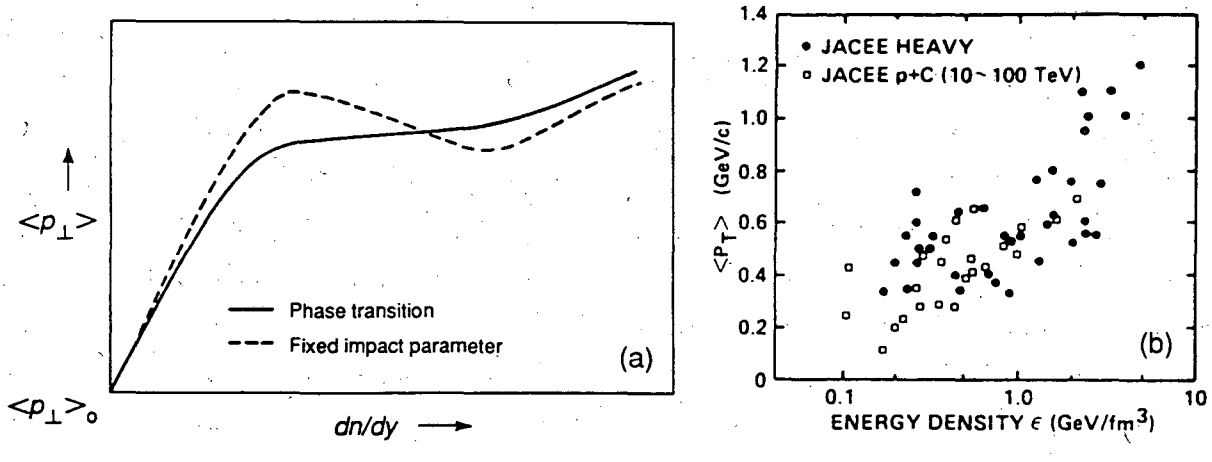

Figure 1. a) The mean transverse momentum $<p_t>$ plotted as a function of the multiplicity density expected from a phase transition in the central baryon-free region of hadronic collisions. The dashed curve corresponds to collisions at a fixed impact parameter. b) The mean transverse momentum $<p_t>$ of photons and π^0 mesons plotted as a function of the energy density, derived from the multiplicity density, measured in high energy cosmic-ray nucleus-nucleus interactions.

rise once all the matter is transformed into the higher temperature state. Therefore, if a QGP phase transition occurs, a plot of the mean transverse momentum as a function of the multiplicity or energy density may exhibit the phase transition curve depicted in Fig. 1a.

Very high energy cosmic ray data[21] taken in nuclear emulsions are displayed in Fig. 1b. Although the data points are widely scattered, the data exhibit characteristics similar to those of a phase transition as depicted in Fig. 1a. The mean transverse momentum $\langle p_t \rangle$ is plotted as a function of the energy density ε derived from the multiplicity density in the emulsion data. These transverse momenta and energy densities start at those measured in pp and $\bar{p}$ p interactions and extend to values of over 1 GeV/c and several GeV/fm^3, respectively. Data from the WA80 experiment using the CERN SPS show similar behavior.[22] However, it was concluded from the data[23] that impact parameter effects in the nucleus-nucleus collision geometry severely complicate any representation of the data in terms of the variables suggested in Fig. 1a. The E735 experiment at the FermiLab Tevatron Collider has produced an analogous plot[24] from $\bar{p}$p data at $\sqrt{s} = 1.8$ TeV, shown in Fig. 2. These data have been interpreted in terms of a phase transition with hydrodynamic flow[25] and in terms of the effects of mini-jets.[26] The spectra may be complicated by many processes.[27]

Components of the Spectrum

The transverse mass (m_t) distributions of produced particles, which are mainly pions, have the potential of providing information on the freezeout temperature in the low m_t part of the spectrum ($m_t < m_\pi$), hydrodynamical flow effects at $m_t \sim m_\pi$, and the primordial critical temperature[20] of the system prior to expansion and freezeout at high m_t ($m_t >> m_\pi$). In the absence of flow effects the low m_t part of the spectrum should reflect the freezeout

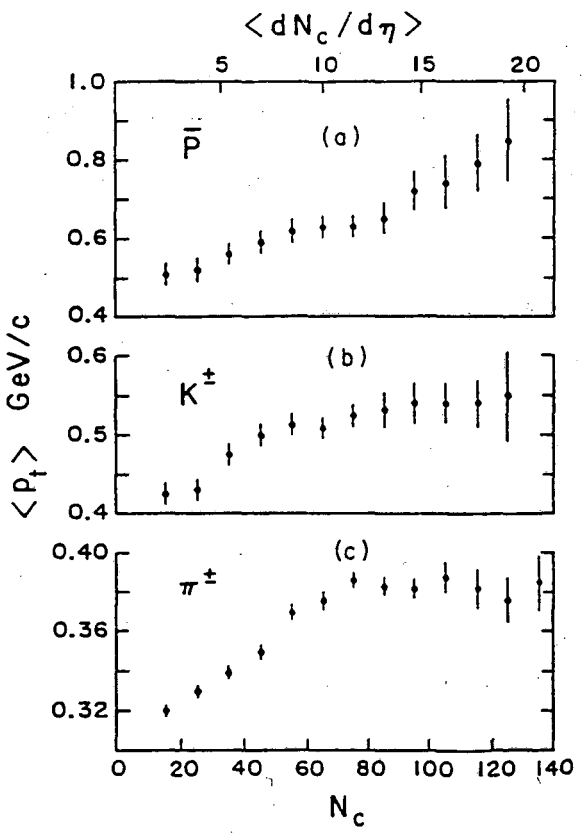

Figure 2. The mean transverse momentum $\langle p_t \rangle$ of a) antiprotons, b) charged kaons and c) charged pions with $p_t < 1.5$ GeV/c, plotted as a function of the charged multiplicity density and measured in $\bar{p}$p interactions at $\sqrt{s} = 1.8$ TeV.

conditions. However, hydrodynamical flow would tend to distort the spectrum and these flow effects might be identifiable in the m_t distributions for various types of particles and colliding systems. Displayed in Fig. 3 are transverse mass distributions, where $m_t = \sqrt{(p_t^2 + m^2)}$, for particle types measured at midrapidity for central collisions of 200 GeV/n O + Au and S + S.[28] Plotted is the variable $m_t^{-3/2} dn/dm_t$ as a function of m_t. Using relativistic thermodynamics as developed by Hagedorn[29] for a single isotropic fireball, a Boltzmann distribution after integration over rapidity gives $dn/dm_t = \kappa\ m_t^{3/2} \exp(-m_t/T)$ for large m_t/T, where κ is a constant. Thus at large m_t, $m_t^{-3/2} dn/dm_t$ plotted as a function of m_t should be a negative exponential with a single slope and temperature T for all particles. This appears to be the case for the measured Λ, K_0 and proton distributions as well as the large m_t regime of the π^- spectra. The straight lines in Fig. 3 correspond to $dn/dm_t = \kappa\ m_t^{3/2} \exp(-m_t/T)$ with T = 200 MeV. Can this be the critical transition temperature that we are seeing?

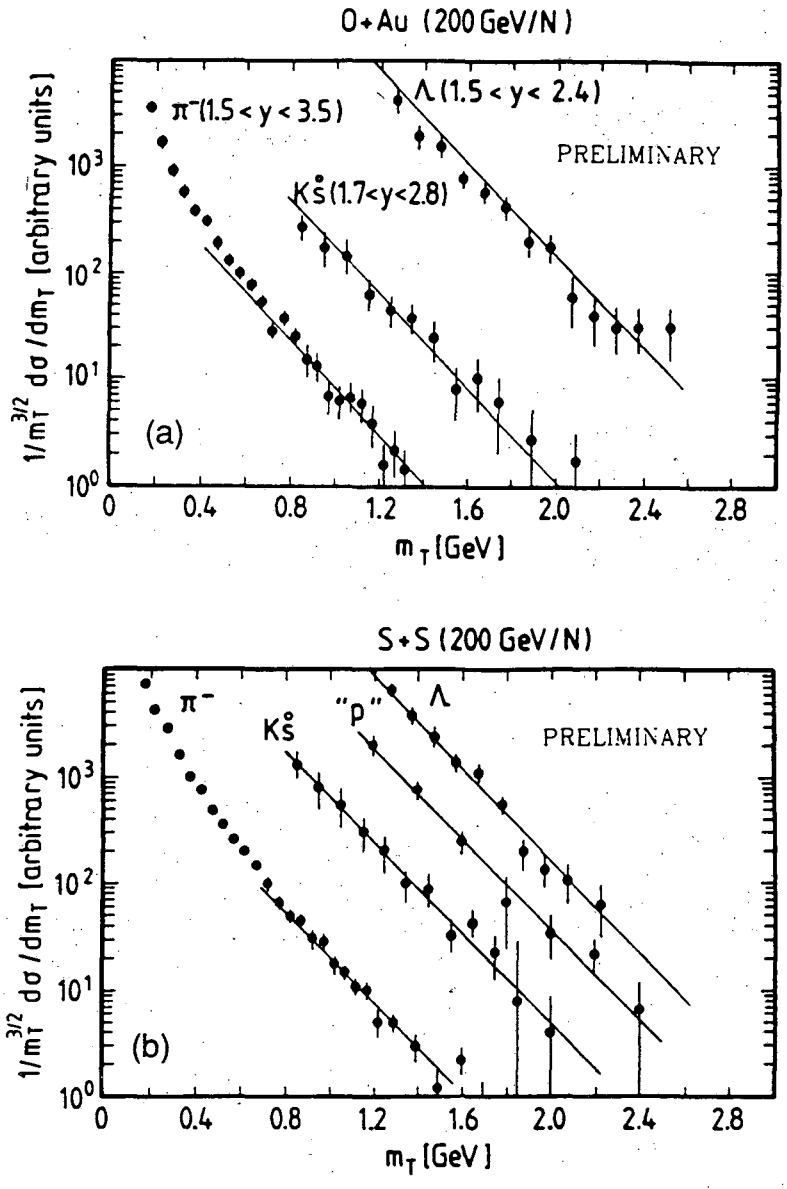

Figure 3. Transverse mass distributions for particles in central collisions of 200 GeV/n a) O + Au and b) S + S. The rapidity intervals for a) are labeled and those for b) are $0.8 < y < 2.0$, $1.5 < y < 3.0$, $1.4 < y < 2.7$ and $1.5 < y < 3.5$ for Λ, p, K^0 and π^-, respectively. The straight lines correspond to a temperature of 200 MeV in the Hagedorn fireball model.

The measured proton and anti-proton spectra from the AGS and SPS do not follow a general trend.[27] They are rapidity-dependent, p_t range-dependent and dependent upon the mass of the colliding nuclei. On the otherhand, the slopes of the m_t spectra of produced particles, represented by T_0, measured at the AGS and SPS have the general characteristic $T_0(K^+) > T_0(K^-) > T_0(\pi)$.[27] This general trend has also been observed in the K^+, K^- and $\pi^{+,-,0}$ spectra measured at the Bevalac and SIS. The important role that resonance production plays in the emitted-particle spectra and its connection with the trend of the slopes of the produced particle spectra will be developed below.

In the Bevalac π^- spectra for 1.8 GeV/n Ar + KCL $\rightarrow \pi^-$, the importance of resonance production was shown by comparisons[30] of the data to calculations of the intranuclear cascade. In the cascade model, pion production results from the production of Δ resonances via the process $NN \rightarrow N\Delta$, where the $\Delta \rightarrow \pi N$ decay produces pions. Displayed in Fig. 4a are the π^- data and in Fig. 4b the results of the cascade calculation. The measured pion spectrum is well described by this simple production mechanism with the possible exception of a small (5%) component at high pion energy (or p_t).

An investigation into the kinematic details of Δ resonance production via $NN \rightarrow N\Delta$ and decay $\Delta \rightarrow \pi N$ was undertaken.[31] A thermal distribution of Δ's with mass m_Δ at temperature T_Δ were generated and then allowed to decay isotropically in the Δ rest frame. The pion and nucleon spectra originating from this process were then fitted using a Boltzmann distribution and the resultant temperatures of the pion and nucleon (proton) are

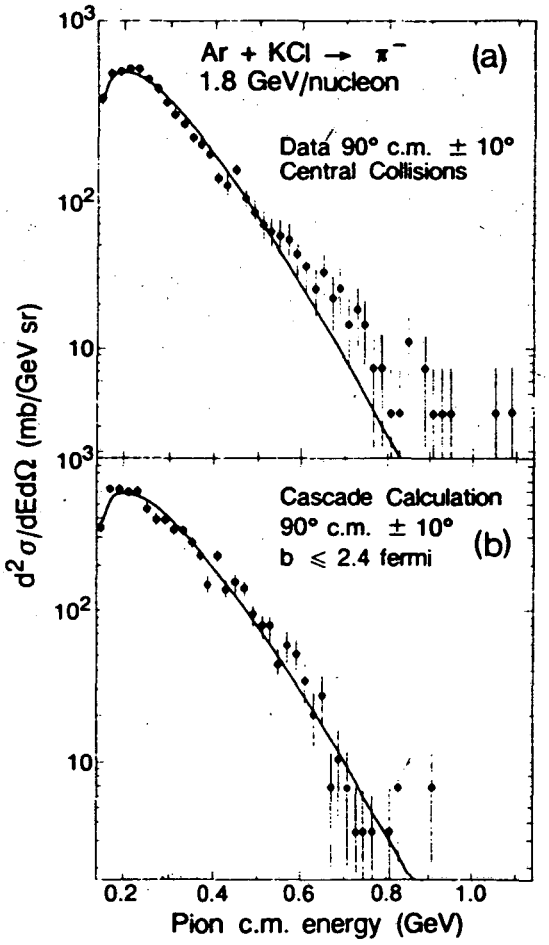

Figure 4. The energy spectrum of negative pions at 90° in the c.m. system a) measured and b) calculated using the intranuclear cascade model. The solid curves are fits to the spectra using a Maxwell-Boltzmann distribution with pion temperatures a) $T_\pi = 69$ MeV and b) $T_\pi = 73$ MeV.

plotted in Fig. 5 as a function of T_Δ. The pion temperatures are lower than the nucleon temperatures and only weakly sensitive to T_Δ, whereas the nucleon temperatures are strongly dependent upon T_Δ. Thus, for purely kinematic reasons the lighter products of the decays of resonances will generally have a lower apparent temperature than the heavier ones.

Further studies of the π^- spectra for heavier colliding systems, La + La[32] and Au + Au,[33] at various energies yield the same basic component at low p_t, namely $NN \rightarrow N\Delta$ with $\Delta \rightarrow \pi N$ as the primary component of the spectra.[34] The higher p_t component, represented by a higher slope parameter, is observed to become increasingly important as the beam energy and/or the masses of the colliding nuclei increase. The origin of this second component is not yet precisely known. Explanations range from pion production from a hot, thermalized source to the influence of collective nuclear flow on the Δ and its subsequent effect on the decay pion spectra.

K^+ and K^- spectra have also been measured at the Bevalac in the reactions 2.1 GeV/n Si + Si $\rightarrow K^-$,[35] and 2.1 GeV/n Ne + NaF $\rightarrow K^+$.[36] The slope parameters measured for these two reactions are $T_0 = 95$ MeV [37] and $T_0 = 122$ MeV, respectively. The K^- spectra have a lower slope parameter than the K^+ spectra. Therefore, the measured slopes at the Bevalac have the same general trend as measured recently in the AGS and SPS experiments, namely $T_0(K^+) > T_0(K^-) > T_0(\pi)$. Also note that the K^- can be produced via resonance production and decay ($NN \rightarrow NY^*$, $Y^* \rightarrow K^-N$), whereas the K^+ has no strong resonance channels and is produced at these energies primarily via associated production, $NN \rightarrow NK\Lambda$. For K^- production the kinematics of the resonance production process and subsequent decay, $NN \rightarrow NY^*$ and $Y^* \rightarrow K^-N$, are analogous to the kinematics of the resonance production and decay process for π production, $NN \rightarrow N\Delta$ and $\Delta \rightarrow \pi N$. From these kinematics the spectrum of the lighter decay particle K^- will have less kinetic energy in the laboratory system than that of the directly produced K^+. This results in a lower T_0 and gives the trend of slopes T_0 that is observed in the spectra for the various particles. Clearly to better understand the role of resonance production in the final state particle spectra at the various energies, extensive calculations which include the resonances and their decay processes are necessary.[38]

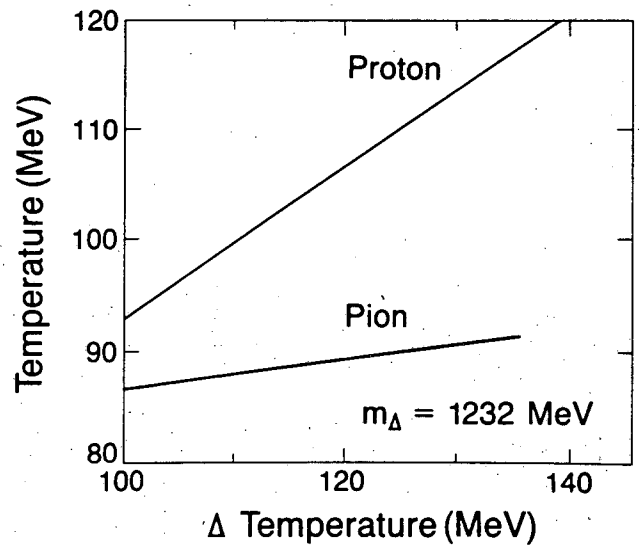

Figure 5. The dependence of the pion and proton apparent temperatures, slope parameters using a Boltzmann fit to the spectra, as a function of the temperature of the parent Δ resonance spectrum assuming $m_\Delta = 1232$.

Flow will have a larger effect on the spectrum of heavier particles than on that of lighter particles. For an ensemble of particles initially at the same temperature, i.e. kinetic energy, the heavier particles will travel at slower thermal velocities. Since the flow velocity and the thermal velocity are additive, in the presence of flow the heavier particles with lower thermal velocities will be affected more strongly than the lighter ones. This has been observed in the collective flow of nuclei of various masses emitted in collisions of heavy nuclei at the Bevalac.[39,40] Therefore, the effect of flow on the slopes of the spectra of different particles is to increase the slope parameter T_0 for heavier particles relative to the lighter ones, i.e. T_0 (heavy particle) > T_0 (light particle). This is consistent with the larger slope values measured for kaons than for pions.

The measured m_t distributions of pions are a complicated mixture of the effects of freezeout, flow and possibly a critical temperature. Using the velocity of sound in an ultrarelativistic gas, $c/\sqrt{3}$, an estimate of the m_t regime where hydrodynamic flow will have its largest effect yields $m_t < 1.22\ m_\pi$. Recent analysis[41,42] of negative hadron spectra,[43] primarily pions, from the SPS in a radial flow model concludes that the spectra can be fit with an average radial flow velocity of $\beta = 0.43c$ and a freezeout temperature of 112 MeV. The initial temperature in this model before expansion is 200 MeV, similar to that derived from the high m_t part of the particle spectra of Fig. 3. A detailed discussion of the effects of flow and comparisons to data can be found in Ref. 44.

The general features of the m_t distributions for the produced particles are surprisingly well reproduced by the radial flow model. Although details of the spectra can be reproduced by the model, they may actually have more complicated origins. Displayed in Figs. 6a and b are ratios of O + Au and p + Au data[43] with respect to minimum bias p + p data[45] as a function of transverse momentum p_t. An enhancement at low and high p_t, i.e. $p_t < 0.2$ GeV/c and $p_t > 1.0$ GeV/c, is observed in both systems. The p_t distribution for p + Au in central collisions exhibits effects which must have similar origin and interpretations as in the O + Au data. These effects in the ratios plotted in Figs. 6a and b have also been observed in very high charged-particle multiplicity (N_{ch}) p + p and $\alpha + \alpha$ events at $\sqrt{S_{nn}}$ =

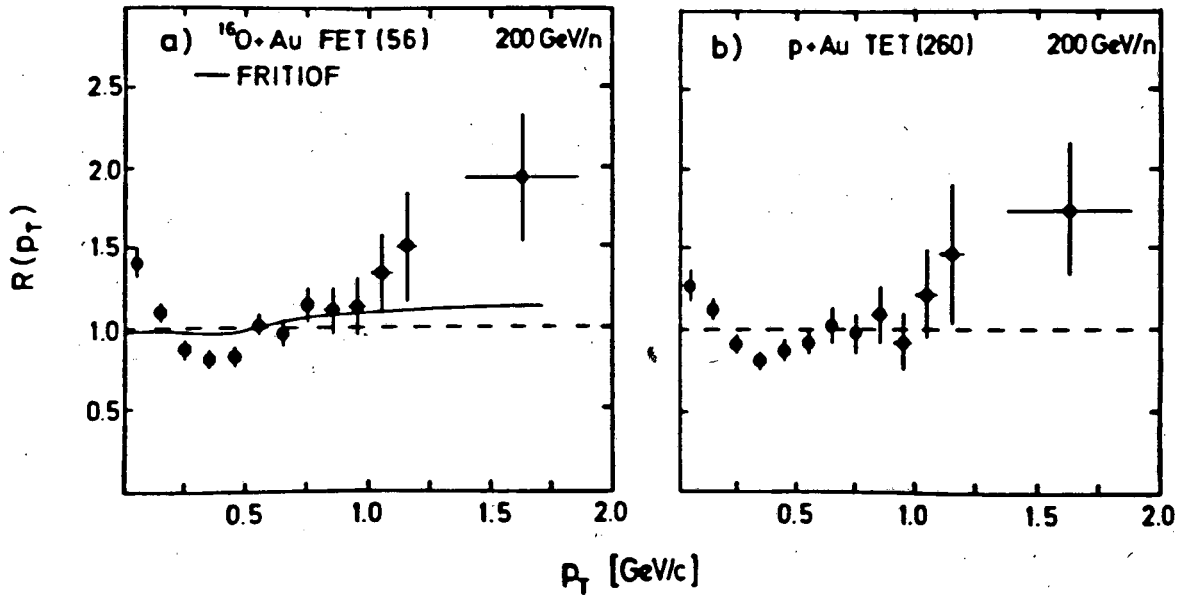

Figure 6. Ratios $R(p_t)$ of the transverse momentum distributions of central a) ^{16}O + Au and b) p + Au collisions relative to minimum bias p + p collisions at 200 GeV/n. The dashed lines indicate $R(p_t) = 1$. The trigger conditions were a) forward energy trigger FET(56) and b) transverse energy trigger TET(260) with trigger cross sections of 56 and 260 mb, respectively.

63 and 31.2 GeV, respectively.[46] These ratios relative to minimum bias data are plotted in Figs. 7a and b for intermediate ($6 \leq N_{ch} \leq 10$) and high ($18 \leq N_{ch}$) multiplicity events. The enhancements at low and high p_t are not observed in the low and intermediate multiplicity data. The structure of the ratios for high N_{ch} events is remarkably similar to those of the central p + Au and O + Au data in Figs. 6a and b. The marked similarity of central p + Au and O + Au collisions to very high multiplicity "hard-scattering" p + p and $\alpha + \alpha$ collisions suggests an explanation may be necessary at the quark-parton level. Similar p_t distributions have been measured in specialized spectrometer experiments for 200 GeV/n nucleus-nucleus collisions in the NA34 experiment at CERN[47] and for $\sqrt{s}$ = 1.8 TeV $\bar{p}p$ in the E735 experiment at FermiLab.[24]

Dielectron Production at the Bevalac to Study In-Medium Processes

Electromagnetic probes such as photons and dileptons interact weakly with the excited matter (nuclear, hadronic or QGP) created in relativistic nucleus-nucleus interactions and therefore can be used as a messenger from this hot, dense matter created in these collisions. At higher collision energies dilepton production may provide a signature[48,49] for the existence of a QGP or can be used to study changes in resonance production[50,51] due to chiral symmetry restoration. In the Bevalac energy regime, dielectron production can be used to study the pion dispersion relation[11,52] or the effects of the medium on the mass and propagation of mesons and resonances.[53,54,55]

Initial experiments have been able to measure dielectron yields in pA interactions[56] down to 13 GeV/c incident beam momentum and in πp interactions[57] down to 16 GeV/c. Measurements at 0.8 GeV/c incident momentum in the pp system[58] were unable to identify any direct electrons down to the level of $e/\pi \leq 3 \times 10^{-6}$. Measurements by the Dilepton Spectrometer Group at the Bevalac have been able to identify dielectron signals in pA[59,60] and AA[61] collisions in the energy range from 1.0 GeV/nucleon to 4.9 GeV/nucleon. At these energies the dominant e^+e^- production processes in the elementary nucleon-nucleon interactions are

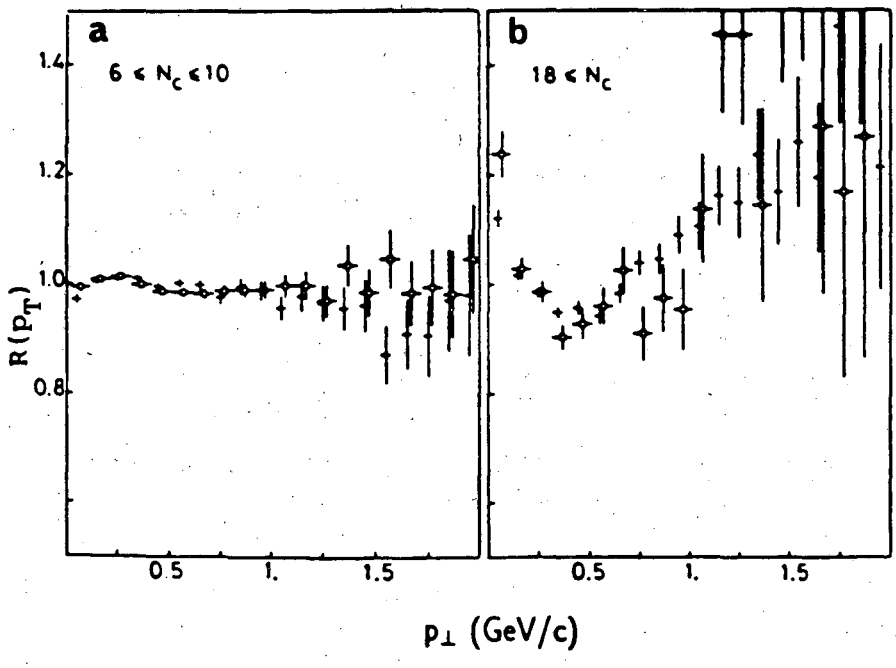

Figure 7. Ratios $R(p_t)$ of the transverse momentum distributions of selected charge multiplicity (N_{ch}) in p + p and $\alpha + \alpha$ events at $\sqrt{S_{nn}}$ = 63 and 31.2 GeV, respectively, relative to minimum bias data for a) intermediate ($6 \leq N_{ch} \leq 10$) and b) high ($18 \leq N_{ch}$) multiplicity events.

pn Bremsstrahlung: $pn \rightarrow pn\gamma \rightarrow pne^+e^-$

and

Dalitz decay: $\Delta \rightarrow Ne^+e^-$
$\eta \rightarrow \gamma e^+e^-$
$\pi^0 \rightarrow \gamma e^+e^-$.

It is expected that dielectrons produced in central nucleus-nucleus collisions may provide information on the temperature and density of the matter in these collisions. In nucleus-nucleus collisions the following annihilation processes enable the study of the effects of the medium on the pion propagation:

πN annihilation: $\pi N \rightarrow N\gamma^* \rightarrow Ne^+e^-$

$\pi\pi$ annihilation $\pi\pi \rightarrow \gamma^* \rightarrow e^+e^-$.

The invariant mass spectrum of dielectrons measured in 1 GeV/n Ca + Ca interactions is displayed in Fig. 8 superimposed with the results of a microscopic BUU calculation.[62] A comparison of the calculations with the 1 GeV/n Ca + Ca data suggest that $\pi\pi$ annihilation dominates in the mass region m > 0.5 GeV and that pn bremsstrahlung and Δ Dalitz decay are important for m < 0.5 GeV. A similar comparison of 1.05, 2.1 and 4.9 GeV p + Be data[60] with calculations of dielectron production in a cascade model[63] concludes that dielectron production from pn bremsstrahlung is the most important process, whereas the Δ Dalitz decay is not important in the p + Be reactions.

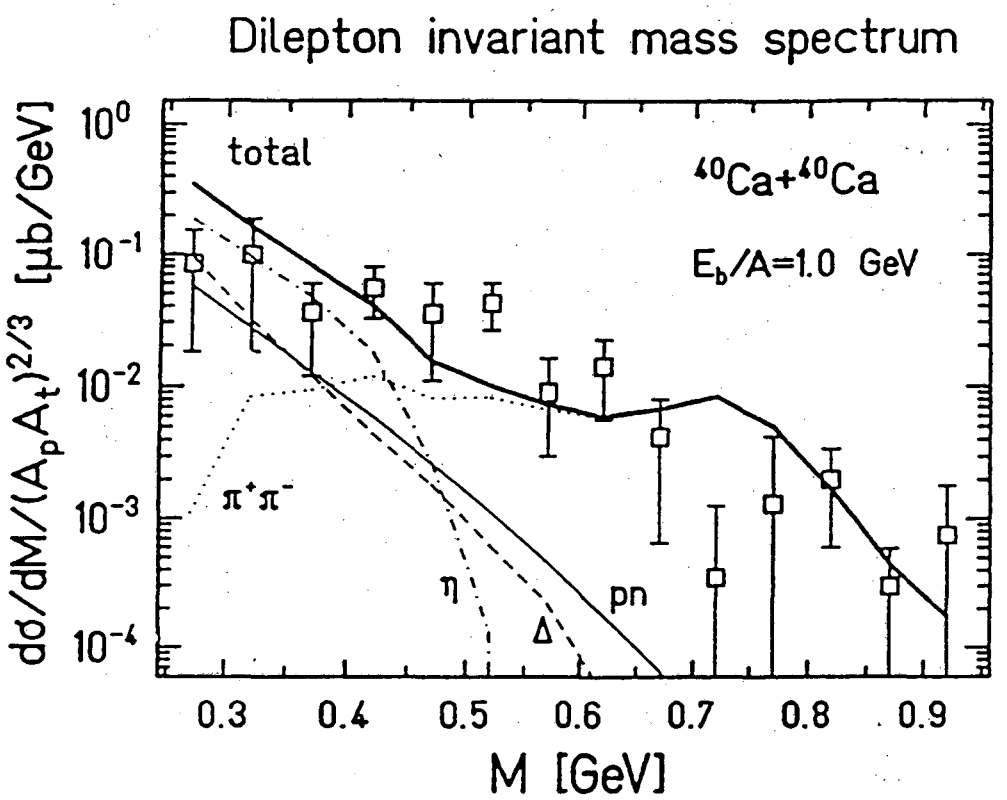

Figure 8. The invariant mass distribution for dielectrons measured in 1 GeV/n Ca + Ca collisions. Shown are the various components which make up the spectrum calculated in a microscopic BUU model (see text):pn bremsstrahlung (solid), πN bremsstrahlung (dot-dashes), $\pi\pi$ annihilation (dots) and Δ decay (dashes). The thick solid line is a sum of all components of the spectrum.

In an attempt to understand the elementary production mechanism for dielectrons, dielectron yields were recently measured in pp and pd interactions[64] at 4.9 GeV/c. A comparison of the pp and pd production should determine whether pn bremsstrahlung plays a dominant role in the dielectron production process. The ratio of the dielectron yield in pd versus pp interactions was measured to be 1.92 ± 0.06. This indicates that the pn bremsstrahlung process is not a dominant source of dielectrons at these energies contrary to the conclusions derived from the comparisons of microscopic calculations and data. Furthermore, the electrons expected from hadronic decays of the η, ρ, ω and Δ resonances in 4.9 GeV pp interactions is compared to dielectron data in Fig. 9.[64] The decays of the hadronic resonances cannot explain the yield or shape of the measured dielectron invariant mass spectrum. This is a topic of extreme theoretical and experimental interest and will require considerable effort to reach an understanding of the mechanism for dielectron production in these reactions.

STOPPING OF NUCLEAR MATTER

The production of a quark-gluon plasma in relativistic heavy ion collisions depends upon whether the energy density reached in the initial phase of the reaction is sufficiently high to initiate a phase transition. Creation of high energy densities requires large energy deposition from the longitudinal motion of the incident nuclei into excitation and transverse degrees of freedom. In terms of bulk properties of nuclear matter the degree to which nuclei can effectively redistribute the initial longitudinal motion into other degrees

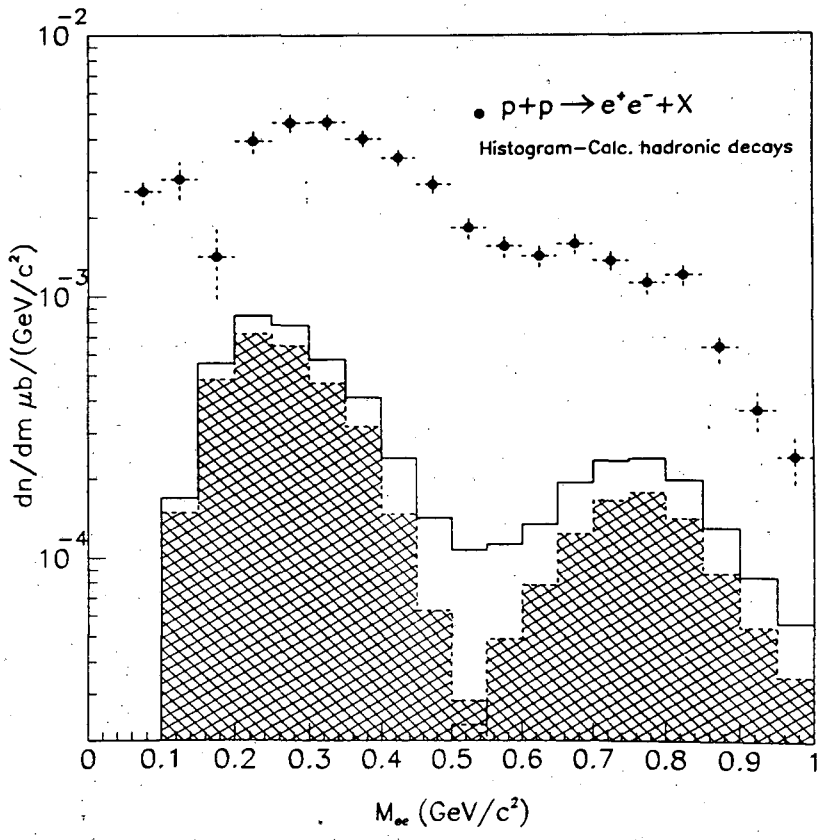

Figure 9. The invariant mass distribution for dielectrons from 4.9 GeV pp interactions. The total calculated electron yield (solid histogram) from the hadronic decays of the η, ρ, ω and Δ resonances is shown for comparison. The hatched areas indicate the individual contributions from the Dalitz decay of the η and the two-body decay of the ω, respectively.

of freedom is referred to as the nuclear stopping power. Rapidity distributions of particles, primordial or produced, and transverse energy distributions provide information on the degree of stopping and the amount of thermalization in the collision process.

The rapidity distributions of particles measured at the Bevalac exhibit complete stopping.[65] This is expected since the total rapidity gap between projectile and target at the highest energy of the Bevalac for nucleus-nucleus collisions is only 1.8 units and the rapidity loss in pA collisions at this and higher energies is typically 1 unit for projectile and target nucleons. Therefore. extrapolation of the Bevalac data to higher energies in order to predict the stopping in nucleus-nucleus collisions is difficult.

Rapidity distributions of the *primordial protons*, originally in the incident nuclei, provide direct information on the degree of stopping in relativistic nucleus-nucleus collisions. Comparisons[66] of the proton rapidity distributions from 14.6 GeV/n Si + Al collisions[67] at the AGS with those of 200 GeV/n S + S collisions[68,69] from the SPS exhibit startling similarities. The mean rapidity losses for the protons in the collisions are approximately the same at the two energies. The rapidity distribution of protons from S + S central collisions exhibits considerably more stopping than predicted in the Lund/FRITIOF model which underpredicts the proton yield at rapidity $y = y_{cm} = 3$. The VENUS 2 string model[70] is successful in predicting the proton rapidity distribution. The main difference in the two models is the inclusion of breakup of leading diquarks in VENUS 2. Relativistic quantum molecular dynamics (RQMD)[71] calculations are also successful in reproducing the measured proton rapidity distributions. Calculations using RQMD and VENUS 2 predict considerable stopping and no baryon-free region at midrapidity for central Au + Au collisions at the SPS and RHIC.[72]

The peak positions of the *rapidity distributions of produced particles* are consistent with a simple geometrical overlap picture of the collision.[73,74] The distributions are Gaussian in shape and are broader than expected for emission from an isotropic fireball.[75] Whether the rapidity distributions represent a large degree of stopping in the Landau[76] sense or partial stopping as predicted by string mechanisms in the Lund/FRITIOF model[77] is still under intense investigation.[78] Thus far, string models and variations[79] of the Landau hydrodynamical model are able to predict the measured rapidity distributions of produced particles at CERN energies.

THE RELATIVISTIC HEAVY ION COLLIDER

Lattice QCD predictions[80,81,82] exhibit a phase transition from hadronic matter to a plasma of deconfined quarks and gluons, the quark-gluon plasma (QGP), at a temperature near 250 MeV. This phase of matter must have existed shortly after the Big Bang and may exist in the cores of dense stars. An important question is whether this predicted state of matter can be created and studied in the laboratory.

The Relativistic Heavy Ion Collider (RHIC)[83,84] is being constructed at Brookhaven National Laboratory to address this question. A schematic diagram of the RHIC accelerator complex is displayed in Fig. 10. Nuclear beams are accelerated from the tandem Van de Graaff accelerator through a transfer line into the AGS Booster synchrotron and into the AGS, which serves as an injector for RHIC. RHIC will accelerate nuclei over a range of energies. Fig. 11 summarizes the capabilities of the accelerator. Completion of the RHIC accelerator and operation for experiments is planned for 1997. In addition to the colliding beams described in Fig. 11, there is a proposal[85] to inject and accelerate polarized protons at RHIC in order to study the spin content of the proton.

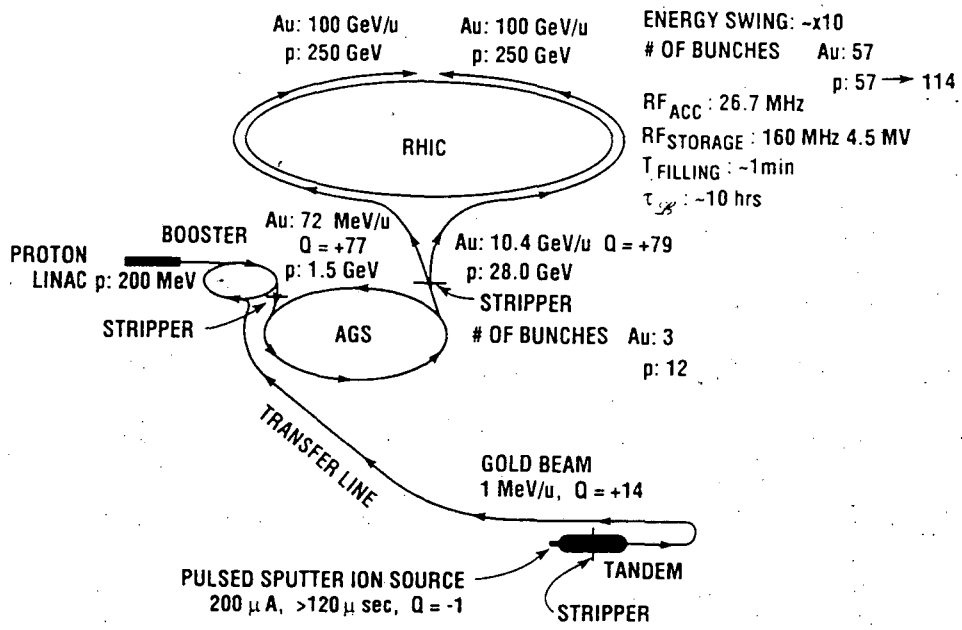

Figure 10. Diagram of the Relativistic Heavy Ion Collider (RHIC) accelerator complex. Nuclear beams are accelerated from the tandem Van de Graaff, through the transfer line into the AGS Booster and AGS prior to injection into RHIC. Some details of the characteristics of proton and Au beams are also indicated after acceleration in each phase.

RHIC EXPERIMENTS

Collisions of the heaviest nuclei at impact parameters near zero are expected to produce approximately 1000 charged particles per unit pseudorapidity at RHIC.[86] This presents a formidable environment in which to detect the products of these reactions. The experiments will take various different approaches to search for the QGP.

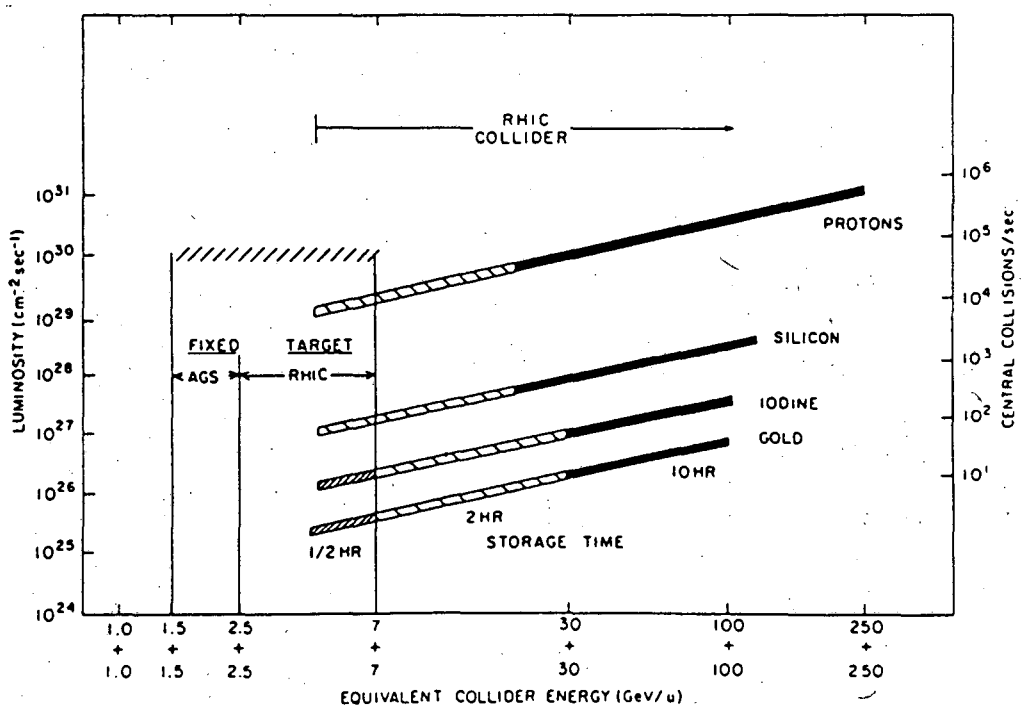

Figure 11. The design luminosity and number of central collisions per second, for impact parameters less than 1 Fermi, are plotted as a function of the colliding beam energies for various projectiles.

At present there are four experiments being considered for the first round at RHIC. There are two large experiments - the Solenoidal Tracker At RHIC (STAR) and the PHENIX experiment - and two smaller ones planned. The STAR experiment will concentrate on measurements of hadron production over a large solid angle in order to perform measurements to study observables on an event-by-event basis. The PHENIX experiment will concentrate on measurements of lepton and photon production as well as have the capability of measuring hadrons. The smaller experiments presently being considered are a forward and midrapidity hadron spectrometer and a compact multiparticle spectrometer (PHOBOS). A brief description of each experiment will be presented along with a more detailed description of STAR.[87]

Forward and Midrapidity Hadron Spectrometer

The physics goals of this experiment[88] are to achieve a basic understanding of relativistic heavy ion collisions at RHIC through a systematic study of AA collisions from the peripheral to the most central in impact parameter. A diagram of the forward and midrapidity spectrometers is shown in Fig. 12. The spectrometers will measure and identify particles, primarily charged π, K and p, and their momenta with high statistics over a small solid angle and over a wide range of rapidity and transverse momentum. This experiment will extract the net baryon densities as a function of rapidity, energy densities and temperatures to determine whether thermal and chemical equilibrium are reached in these collisions. It will also be able to study both high and low transverse momentum processes.

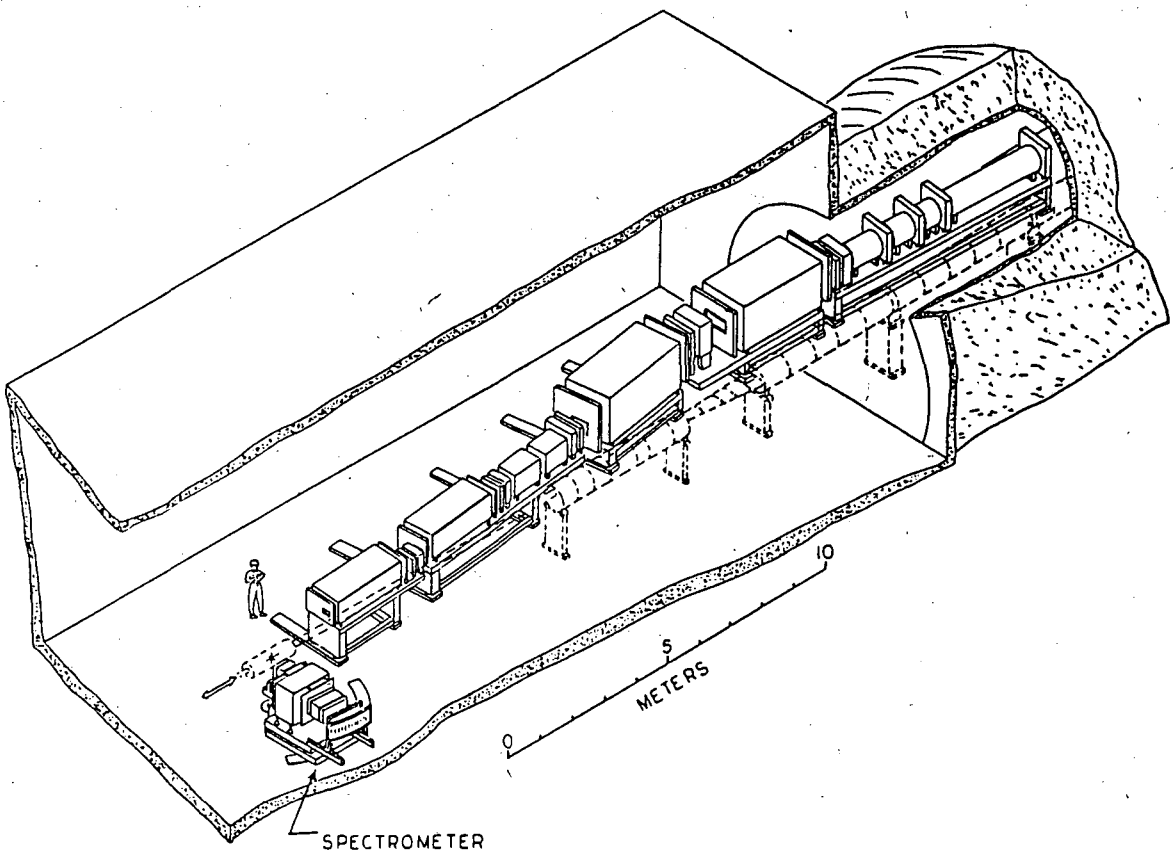

Figure 12. A diagram of the forward and midrapidity spectrometer experiment in the narrow angle hall at RHIC.

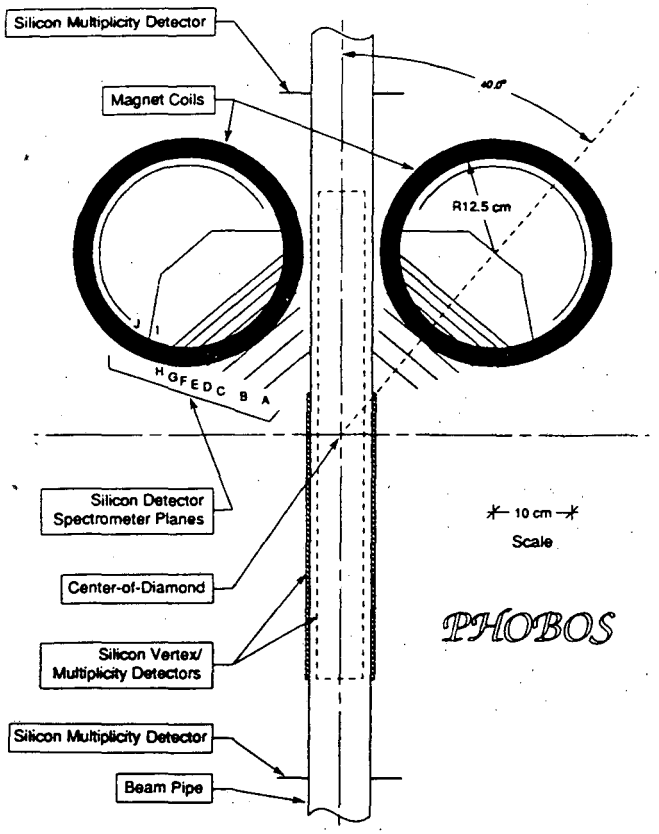

Figure 13. A diagram of the PHOBOS two-arm multiparticle spectrometer. The two arms are located on opposite sides of the beam pipe. Each arm has a 6 Tesla magnet represented by the coils with silicon detector planes for tracking.

The PHOBOS Experiment

The physics goals of the PHOBOS experiment[89,90] are to measure single particle spectra and correlations between particles with low transverse momenta. Charged particles will be measured and identified in the range $0 \leq y \leq 1.5$ and 15 MeV/c $\leq p_t \leq$ 600 MeV/c for pions and 45 MeV/c $\leq p_t \leq$ 1200 MeV/c for protons. The range of particles to be studied include γ, $\pi^{\pm}$, $K^{\pm}$, p, $\bar{p}$, ϕ, Λ, $\bar{\Lambda}$, d and $\bar{d}$. Particle ratios, p_t spectra, strangeness production ($K^{\pm}$, ϕ, Λ, $\bar{\Lambda}$) and particle correlations will be studied. A multiplicity detector will allow the classification of events by global event characteristics. An illustration of the experiment is shown in Fig. 13.

The PHENIX Experiment

The physics goals of PHENIX[91] are to measure as many potential signatures of the QGP as possible as a function of a well defined common variable such as impact parameter or pseudorapidity density. The studies can be divided into three categories: basic QCD phenomena, basic collision dynamics and the thermodynamic features of the initial state.

The variables to be measured are lepton pairs (di-electrons and di-muons), photons and hadrons. The experiment will be sensitive to small cross section processes such as the production of the J/ψ, Υ and high p_t spectra. It will also have the capability for high rates with pp and pA collisions.

A diagram of the PHENIX detector is displayed in Fig. 14. The magnet has an axial field with tracking chambers and detectors for the identification of electrons, muons, photons and hadrons. There are two arms for dielectron measurements with approximately

1 steradian acceptance at midrapidity and a separate forward muon spectrometer as shown in Fig. 14. Photons and hadrons will be measured at midrapidity with approximately 0.5 steradian acceptances.

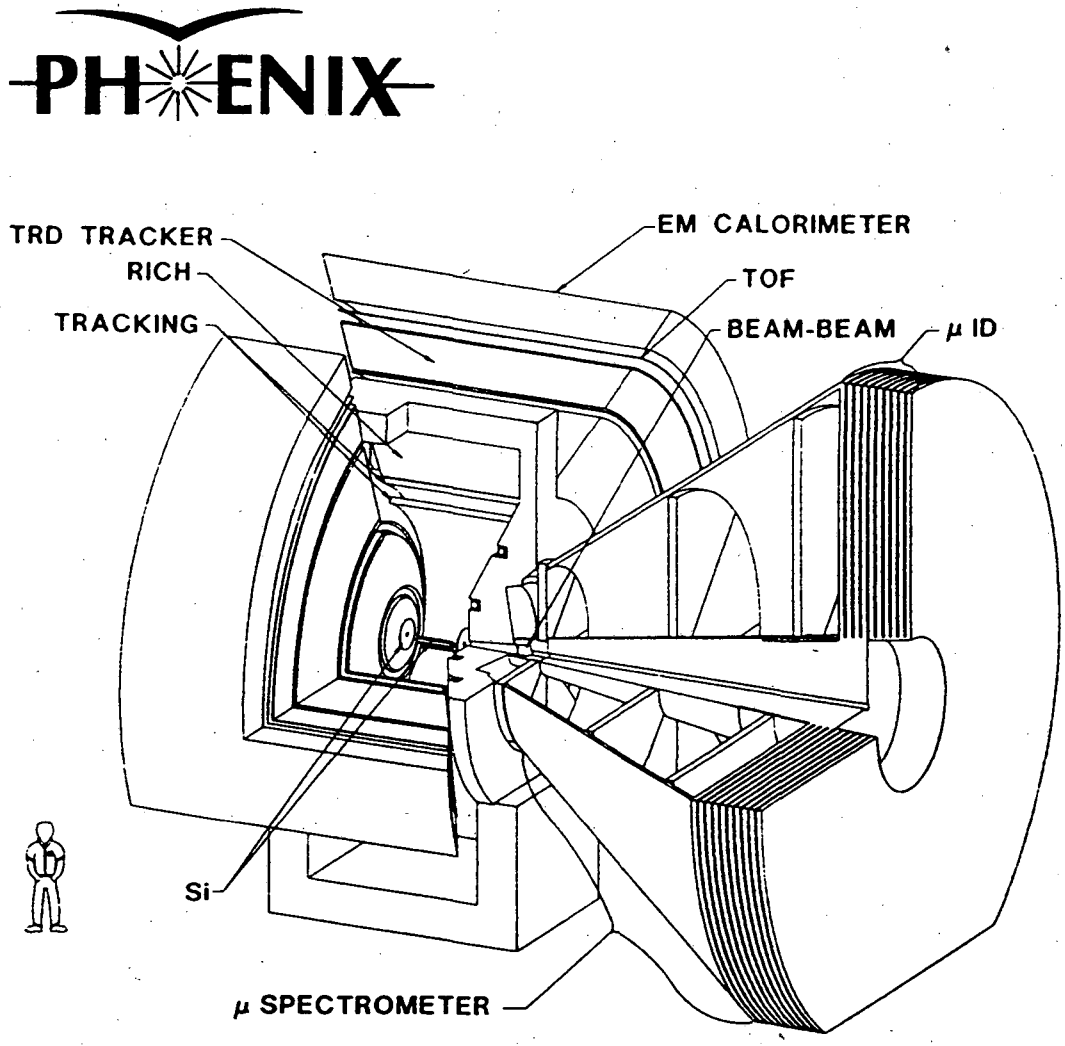

Figure 14. A diagram of the PHENIX experiment at RHIC. The beams collide along the horizontal direction in the center of the detector. The detector components are labeled.

The STAR Experiment

The STAR experiment[92,93,94] will search for signatures of QGP formation and investigate the behavior of strongly interacting matter at high energy density. A flexible detection system will be utilized to simultaneously measure many experimental observables. The experiment will exploit two aspects of hadron production that are fundamentally new at RHIC: correlations between *global observables on an event-by-event basis* and the use of *hard scattering of partons* as a probe of the properties of high density nuclear matter.

The event-by-event measurement of global observables – such as temperature, flavor composition, collision geometry, reaction dynamics, and energy or entropy density fluctuations – is possible because of the very high charged particle densities, $dn_{ch}/d\eta \approx 1000$ expected in nucleus-nucleus collisions at RHIC. This will allow novel determination of the thermodynamic properties of single events. Full azimuthal coverage with good particle identification and continuous tracking is required to perform these measurements.

Correlations between observables will be made on an event-by-event basis to isolate potentially interesting event types.

Measurable yields of high p_t particles and jets at RHIC will allow investigations of hard QCD processes via both highly segmented calorimetry and high p_t single particle measurements. A systematic study of particle and jet production will be carried out over a range of colliding nuclei from p + p through Au + Au, over a range of impact parameters from peripheral to central, and over the range of energies available at RHIC. Measurements of the remnants of hard-scattered partons will be used as a penetrating probe of the QGP, and will provide important new information on the nucleon structure function and parton shadowing in nuclei.

Measurements will be made at midrapidity over a large pseudo-rapidity range ($|\eta| < 2$) with full azimuthal coverage ($\Delta\phi = 2\pi$) and azimuthal symmetry. The detection system is shown in Fig. 15. It will consist of a silicon vertex tracker (SVT) and time projection chamber (TPC) inside a superconducting solenoidal magnet for tracking, momentum analysis and low p_t particle identification via dE/dx; a time-of-flight system surrounding the TPC for particle identification at higher momenta; and electromagnetic calorimetry outside the solenoid to trigger on and measure jets, and to measure the transverse energy of events. The tracking and particle identification are needed mainly to study the low p_t physics, and the calorimetry to study the high p_t physics.

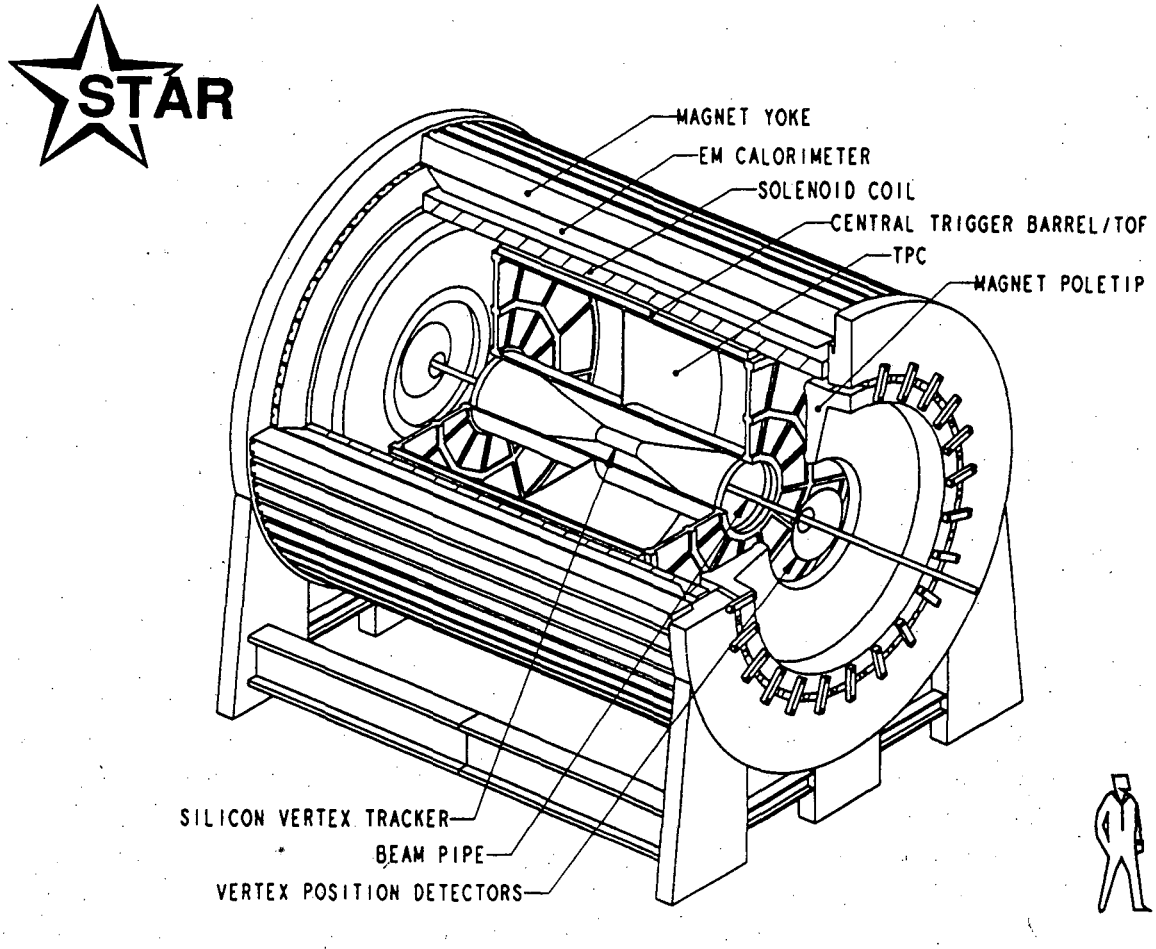

Figure 15. Conceptual layout of the experiment, with cylindrical symmetry around the beam axis. See text for description.

Particle Spectra

As a consequence of the high multiplicities in central nucleus-nucleus events, the slope of the transverse momentum (p_t) distribution for pions and the $\langle p_t \rangle$ for pions and kaons can be determined *event-by-event.* Thus, individual events can be characterized by a slope parameter T_0 or "temperature" to search for events with extremely high temperature, predicted[95] to result from deflagration of a QGP. Displayed in Fig. 16 are two spectra generated by the Monte Carlo method from Maxwell-Boltzmann distributions with T = 150 and 250 MeV, each containing 1000 pions. This is the average number of pions of a given charge sign expected in the acceptance $|\eta| < 1$ of this experiment for central Au + Au collisions. The slopes of spectra with T = 150 and 250 MeV derived from fits using a Maxwell-Boltzmann distribution, also shown in Fig. 16, can easily be discriminated at the single event level. The determination of $\langle p_t \rangle$ for pions can be made very accurately on the single event basis in this experiment, over the expected range of multiplicities in central collisions from Ca + Ca to Au + Au. Even for kaons, with ~ 200 charged kaons per event in the acceptance for central Au + Au events, $\langle p_t \rangle$ can be determined accurately for single events.

Inclusive p_t distributions of charged particles will be measured with high statistics to investigate effects such as collective radial flow[96] and critical temperature[97] at low p_t, and mini-jet attenuation[98,99] at high p_t. The p_t spectra of baryons and anti-baryons at midrapidity are particularly interesting for determining the stopping power of quarks. The difference between the p_t spectra obtained for p and $\bar{p}$ or Λ and $\bar{\Lambda}$ will reflect the redistribution in phase space of valence quarks from the nucleons of the target and projectile. This measurement of the net baryon number and net charge is important for establishing the baryo-chemical potential $\mu_B(y)$ at midrapidity.[100]

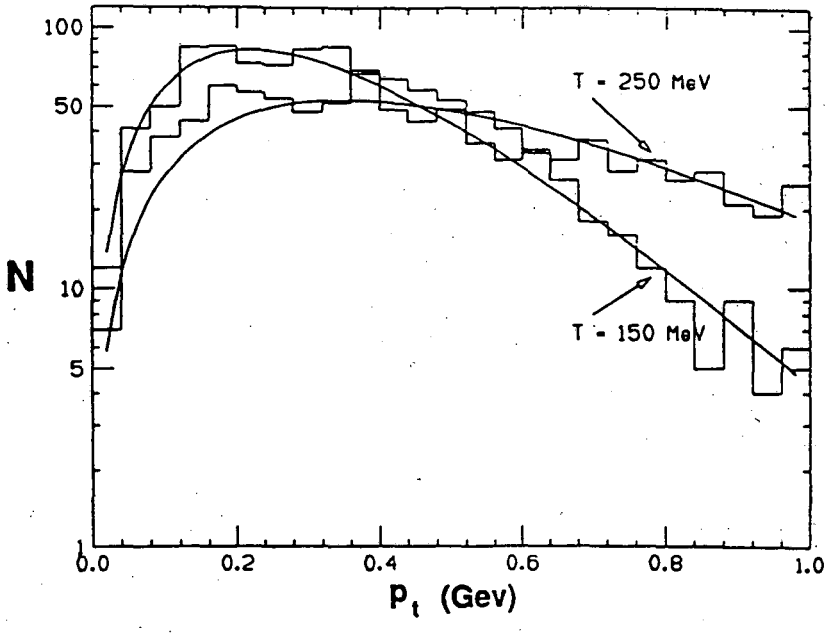

Figure 16. Simulation of the p_t spectrum for one event generated using a Boltzmann distribution of 1000 pions. The histograms correspond to single events generated with T = 150 MeV and 250 MeV. The curves are fits to the histogram using a Maxwell-Boltzmann distribution.

There have been many predictions regarding signatures of the QGP. One of the first predictions of a signature for the formation of a QGP was the enhancement in the production of strange particles resulting from chemical equilibrium of a system of quarks and gluons[101]. A measurement of the K/π ratio provides information on the relative concentration of strange and nonstrange quarks, i.e. $\langle(s + \bar{s})/(u + \bar{u} + d + \bar{d})\rangle$. This has been suggested[102] as a diagnostic tool to differentiate between a hadronic gas and a QGP, and to study the role of the expansion velocity. The K/π ratio will be measured *event-by-event* with sufficient accuracy to classify the events for correlations with other event observables. Another unique feature of STAR is its ability to measure strange and anti-strange baryons (e.g. $\bar{\Lambda}$, Λ, K^o_s) over a wide rapidity interval about midrapidity. Enhancements to the strange antibaryon content due to QGP formation have been predicted.[103] Invariant mass distributions of K^o_s which will be measured in STAR from the decay $K^o_s \rightarrow \pi^+\pi^-$ are shown in Fig. 17. Furthermore, multiply-strange baryons (Ξ^-, $\bar{\Xi}^-$, Ω^-) may be more sensitive to the existence of the QGP.[104] An example of the mass spectrum expected from the decay $\Xi^- \rightarrow \Lambda\pi^-$ with $\Lambda \rightarrow \pi^-p$ in the STAR experiment is shown in Fig. 18.

The production cross section of ϕ-mesons can be measured *inclusively* from the decay $\phi \Rightarrow K^+ + K^-$. Displayed in Fig. 19 is an invariant mass spectrum, in the region of the ϕ mass, constructed from all possible combinations of identifiable K^+ and K^- in the acceptance $|\eta| < 1$. The momentum resolution and tracking efficiencies of the STAR tracking system are included in the simulation. The mean number of reconstructed ϕ's in Au + Au central events at RHIC is 6 per event in the STAR detector. Measurement of the yield of the ϕ, which is an $s\bar{s}$ pair, places a more stringent constraint on the origin of the observed flavor composition[105] than the K/π ratio and is expected to be more sensitive to the presence of a QGP. The ϕ production rate is also expected to be extremely sensitive to changes in the quark masses[106,107,108] due to a chiral phase transition at high energy densities, which is predicted in lattice QCD calculations.[109,110]

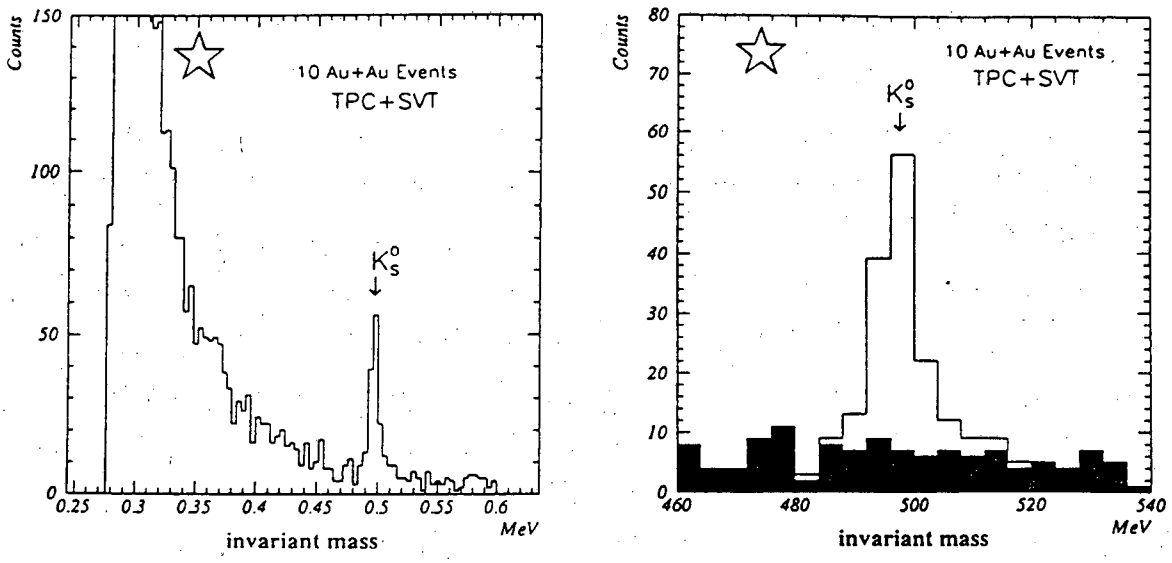

Figure 17. Simulated invariant mass distribution for $K^o_s \rightarrow \pi^+\pi^-$ measured in STAR for 10 central Au + Au events at RHIC. The right-hand side is an expanded view in the region of the K^o_s mass. The shaded area represents the contribution from random combinatorial background.

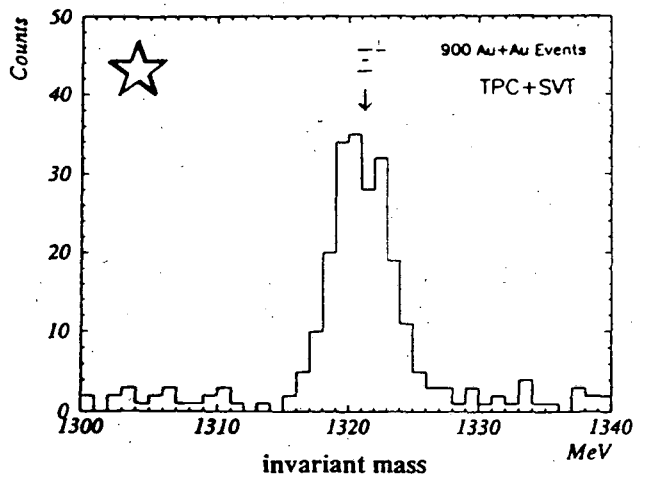

Figure 18. Simulated invariant mass distribution from the decay $\Xi^- \rightarrow \Lambda\pi^-$ with $\Lambda \rightarrow \pi^- p$ measured in STAR for 900 central Au + Au events at RHIC.

Hanbury-Brown and Twiss (HBT) Interferometry

Correlations between identical bosons provide information on the freezeout geometry,[111] the expansion dynamics[112] and possibly the existence of a QGP.[113] It would be unprecedented to be able to measure the pion source parameters via pion correlation analysis on an *event-by-event* basis and to correlate them with other event observables. In an individual event with 1000 negative pions within $|\eta| < 1$, the number of $\pi^-\pi^-$ pairs is $n_{\pi^-}(n_{\pi^-}-1)/2 = 500{,}000$. The two-pion correlation statistics for a single central Au + Au event at RHIC will be similar to the accumulated statistics published in most papers on the subject. An empirical relation for the transverse radius (R_t) of the pion source at midrapidity as a function of the rapidity density (dn/dy) has been derived from the existing

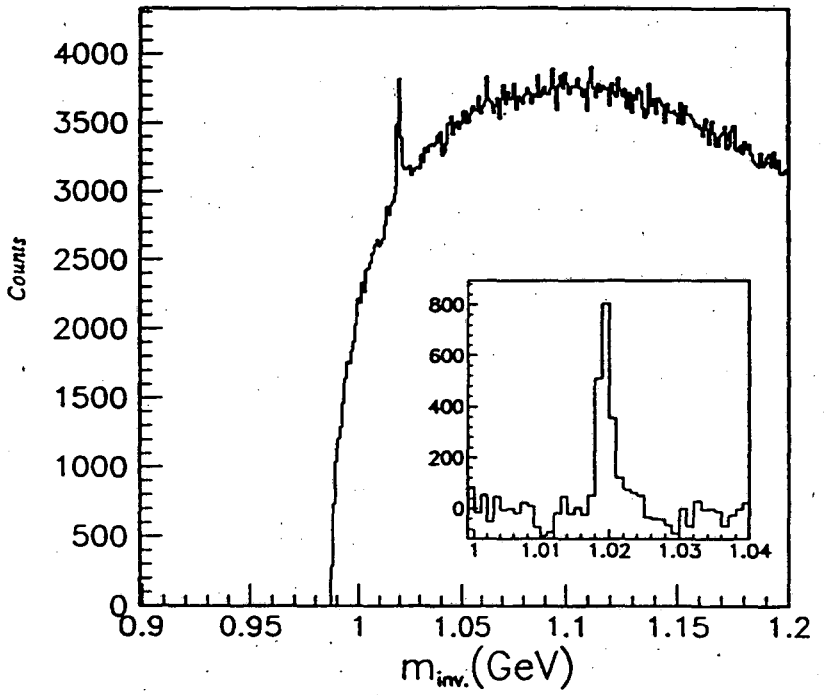

Figure 19. Invariant mass distribution for all identifiable K^+K^- pair combinations simulated in the acceptance $|\eta| < 1$ of STAR for 500 Au + Au central events at RHIC. The ϕ signal is the narrow peak at 1.02 GeV. The inset is the result of a subtraction of K^+K^- pairs formed from K^+ and K^-, each from a different event, from the true K^+K^- pairs of the main part of this figure. The simulation has no width for the ϕ and the contribution of the detector to the measurement of the ϕ is observed to be minimal compared to the true width of $\Gamma = 4.4$ MeV.

pion correlation data[114] shown in Fig. 20. This relation, $R_t \sim (dn/dy)^{-1/3}$, suggests that rather large source sizes, $R_t \sim 10$ fm, will be measured in central Au + Au collisions at RHIC. An example of a simulated correlation measurement in STAR for a single Au + Au central collision event at RHIC is shown in Fig. 21.

The correlations of like-sign charged kaons or pions will be measured on an *inclusive* basis to high accuracy. The dependence of the source parameters on the transverse momentum components of the particle pairs will be measured with high statistics. Measurement of correlations between unlike-sign pairs will yield information on the Coulomb corrections and effects of final state interactions. The *inclusive* measurement of KK correlations will complement the $\pi\pi$ correlation data. The KK correlation is less affected by resonance decays after hadronic freeze-out than the $\pi\pi$ correlations[115], thus interpretation of the KK correlation measurements is much less model-dependent than that of the $\pi\pi$ data. Since K's are expected to freeze out earlier[116] than π's in the expansion, the K source sizes are expected to be smaller than those of the π's. Depending upon the baryo-chemical potential and the existence of a QGP, the K^+ and K^- are also expected to freeze out at different times. Thus, separate measurements of the K^+K^+ and K^-K^- correlation functions will be of interest.

Electromagnetic Energy

One-third of the energy produced at midrapidity in these collisions will be electromagnetic (EM) energy. The hadronic energy can be measured by charged particle tracking. The EM energy must be measured using calorimetry. The measurement of EM energy vs. charged-particle energy is an important correlation to measure in the search for the QGP and other new physics. The unexplained imbalance between charged particle and neutral energy observed in Centauro and other cosmic ray events emphasizes the need for EM/charged particle measurements.[117] Discussions of quark-gluon scattering within the QGP (e.g., $qg \rightarrow \gamma q$) also point to the importance of measuring the electromagnetic energy as a possible signature of special events.[118]

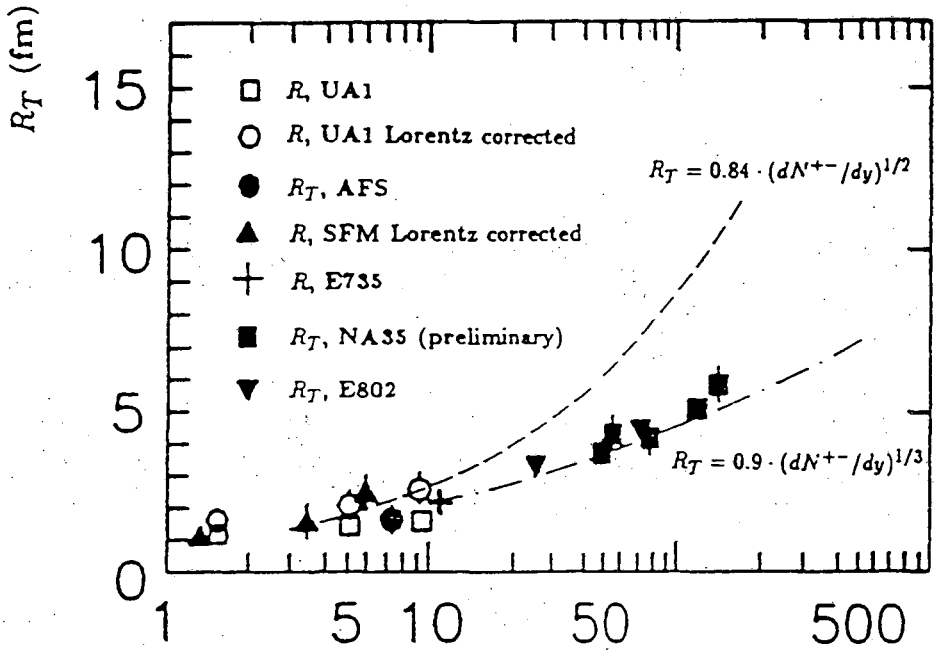

Figure 20. The correlation between the transverse source radii, derived from two-pion correlation measurements, and the charged-particle rapidity density at midrapidity. Measurements from the Sp $\bar{p}$S collider, ISR collider, Tevatron collider, Brookhaven AGS heavy ions and the CERN SPS heavy ions are presented. Two parameterizations corresponding to $R_t \sim (dn/dy)^{-1/2}$ and $R_t \sim (dn/dy)^{-1/3}$ are shown.

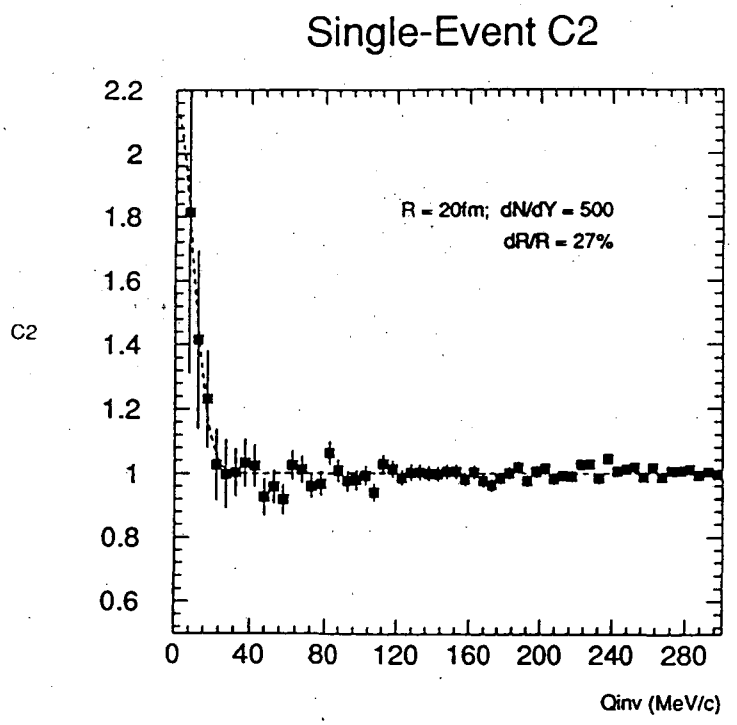

Figure 21. Correlation measurement for a single event simulated with R_{inv} = 20 fm and $dN_{\pi^-}/d\eta$ = 500 in STAR at midrapidity.

Fluctuations in Energy, Entropy, Multiplicity and Transverse Momentum

It has long been known that a prime, general indicator of a phase transition is the appearance of critical dynamical fluctuations in a narrow range of conditions. It is worth emphasizing that such critical fluctuations can only be seen in individual events where the statistics are large enough to overcome uncertainties ($\sqrt{N}$) due to finite particle number fluctuations. The large transverse energy and multiplicity densities at midrapidity in central collisions allow *event-by-event* measurement of fluctuations in particle ratios, energy density, entropy density and flow of different types of particles as a function of p_t, rapidity, and azimuthal angle. They also allow measurements of local fluctuations in the magnitude and azimuthal distribution of p_t. These fluctuations have been predicted to arise from the process of hadronization of a QGP.[119]

Parton Physics from Jets, Mini-Jets and High p_t Single Particles

The goal of studying products of hard QCD processes produced in relativistic heavy ion collisions is to use the propagation of quarks and gluons as a probe of nuclear matter, hot hadronic matter and quark matter. Since the hard scattering processes are directly calculable in QCD, a measurement of the yield of hard scattered partons as a function of their transverse energy should be sensitive to their interaction with the surrounding matter. The partons in a single hard scattering (dijet) whose products are observed at midrapidity must traverse distances of several fermi through high density matter in a nucleus-nucleus collision. The energy loss of these propagating quarks and gluons is predicted[120] to be sensitive to the medium and may be a direct method of observing the excitation of the medium, i.e., the QGP. Passage through hadronic or nuclear matter is predicted to result in an attenuation of the jet energy and broadening of jets. Relative to this damped case, a QGP is transparent and an enhanced yield is expected. The yield of jets will be measured as a function of the transverse energy of the jet. The jet events can also be correlated with

other *event-by-event* observables to deduce information on the dynamics of the collision process.

Mini-jets are expected to be produced copiously in collisions at RHIC.[121,122] As is the case for high p_t jets, the observed yield of mini-jets is expected to be influenced strongly by the state of the high density medium through which they propagate. It is important to study the degree of fluctuation of the transverse energy and multiplicity as a function of rapidity and azimuthal angle ($d^2E_t/dyd\phi$ and $d^2n/dyd\phi$) *event-by-event*, which should be strongly affected by mini-jets.[123]. The *inclusive* p_t distributions of hadrons at $p_t > 3$ GeV/c will also be influenced by jets and mini-jets as can be seen in Fig. 22.

Correlations between Event Observables

It should be emphasized that the capability of measuring several different observables event-by-event is unique to this experiment. Events can be characterized event-by-event by their temperature, flavor content, transverse energy density, multiplicity density, entropy density, degree of fluctuations, occurrence of jets and possibly source size. The presence of a QGP is not likely to be observed in an average event, nor is it expected to be observed in a large fraction of events. Since there is no single clearly established signature of the QGP, access to many observables simultaneously will be critical for identifying the rare events in which a QGP is formed.

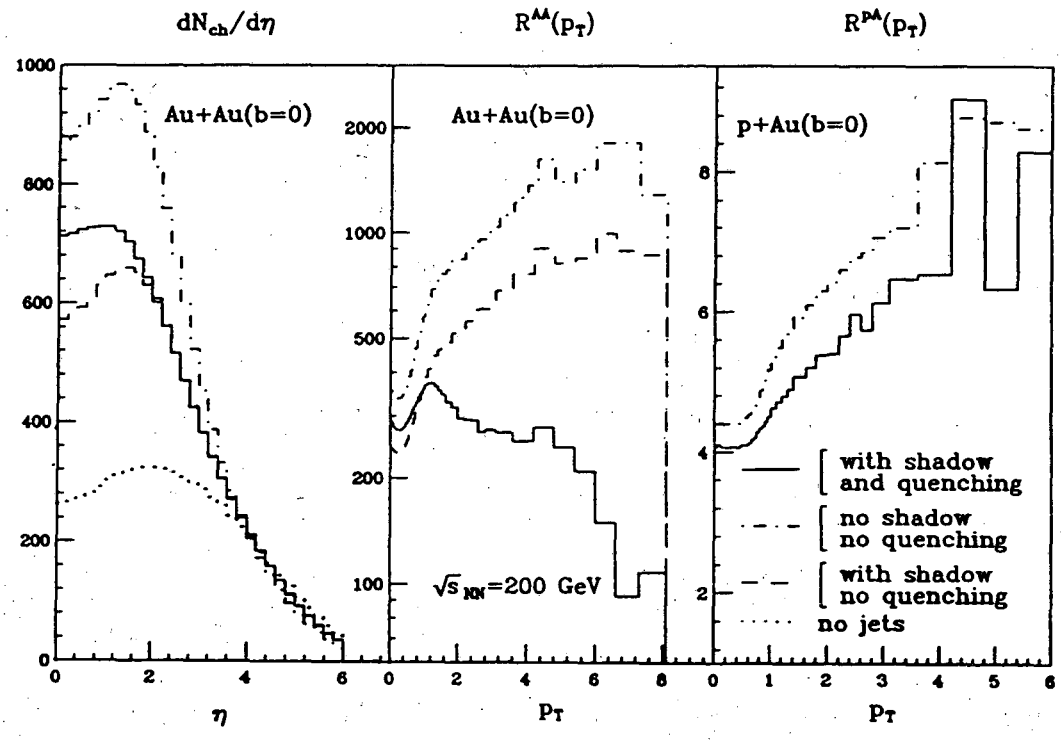

Figure 22. Results from HIJING calculations on the dependence of the inclusive charged hadron spectra in central Au + Au and p + Au collisions on minijet production (dash-dotted), gluon shadowing (dashed) and jet quenching (solid) assuming that the gluon shadowing is identical to that of quarks (see Ref. [124] for details). $R^{AB}(p_t)$ is the ratio of the inclusive p_t spectrum of charged hadrons in A + B collisions to that of p + p.

ACKNOWLEDGEMENTS

I would like to thank the members of the STAR and NA35 Collaborations for their work which is presented in the manuscript. I am especially indebted to S. Margetis, R. Morse and W. Christie for calculations and figures used in these lectures. I thank H. Huang and J. Carroll for their comments and Joy Lofdahl for assistance with the manuscript. This work was supported in part by the Director, Office of Energy Research, Division of Nuclear Physics of the Office of High Energy and Nuclear Physics of the U.S. Department of Energy under contract DE-AC03-76SF00098.

REFERENCES

[1] For the future perspectives utilizing heavy nuclear beams in the Large Hadron Collider, please see the lectures in this School of P. Giubellino.

[2] E. Feenberg and H. Primakoff, Phys. Rev. 70, 980 (1946).

[3] A.R. Bodmer, Phys. Rev. D4, 1601 (1971).

[4] G. Baym and S.A. Chin, Phys. Lett. 62B, 241 (1976).

[5] T.D. Lee and G.C. Wick, Phys. Rev. D9, 2291 (1974).

[6] T.D. Lee, Rev. Mod. Phys. 47, 267 (1975).

[7] In the article above, T.D. Lee points out that "in high-energy physics we have concentrated on experiments in which we distribute a higher and higher amount of energy into a region with smaller and smaller dimensions. In order to study the question of 'vacuum', we must turn to a different direction; we should investigate some 'bulk' phenomena by distributing high energy over a relatively large volume."

[8] J.C. Collins and M.J. Perry, Phys. Rev. Lett. 34, 1353 (1975).

[9] G. Chapline and M. Nauenberg, Phys. Rev. D16, 450 (1977).

[10] L. Susskind, Phys. Rev. D20, 2610 (1979).

[11] A.B. Migdal, Rev. Mod. Phys. 50, 107 (1978) and references therein.

[12] V. Ruck, M. Gyulassy and W. Greiner, Z. Phys. A277, 391 (1976).

[13] See B. Mueller lectures of this School.

[14] K. Geiger and B. Mueller, Nucl. Phys. B369, 600 (1992); see also K. Geiger lecture at this School.

[15] With the exception of the synchophasotron, which cannot accelerate nuclear beams of masses heavier than A = 20.

[16] J. Cugnon, D. Kinet and J. Vandermeulen, Nucl. Phys. A379 (1982) 553; J. Cugnon, T. Mitzutani and J. Vandermuelen, Nucl. Phys. A352, 505 (1981).

[17] B. Andersson, G. Gustafson and B. Nilsson-Almqvist, Nucl. Phys. B281, 289 (1987); B. Andersson et al., Phys. Rep. 97, 31 (1983); B. Nilsson-Almqvist and E. Stenlund, Comp. Phys. Comm. 43, 387 (1987).

[18] H. Gustafsson et al., Phys. Rev. Lett. 52, 1590 (1984).

[19] R.E. Renfordt et al., Phys. Rev. Lett. 53, 763 (1984).

[20] L. Van Hove, Phys. Lett. B118, 138 (1982).

[21] T.H. Burnett et al., Phys. Rev. Lett. 57, 3249 (1986).

[22] R. Albrecht et al., Phys. Lett. B201, 390 (1988).

[23] M. Purscke, Ph.D. Thesis, University of Muenster (1990).

[24] T. Alexopoulos et al., Phys. Rev. Lett. 64, 991 (1990).

[25] P. Levai and B. Mueller, Phys. Rev. Lett. 67, 1519 (1991).

[26] X.N. Wang and M. Gyulassy, Duke University Preprint-TH-91-24 and Lawrence Berkeley Laboratory Report LBL-31538 (1991).

[27] For more details on the spectra see B.V. Jacak lectures of this School.

[28] J.W. Harris and the NA35 Collaboration, Workshop on Nucelar Dynamics VI, Jackson Hole, Wyoming, Lawrence Berkeley Report LBL-28709, 79 (1990).

[29] R. Hagedorn, CERN 71-12 (1971); GSI-Report 81-6, 236 (1981); Proceedings of Quark Matter 84, ed. K. Kajantie, Springer-Verlag, 53 (1985).

[30] R. Brockmann et al., Phys. Rev. Lett. 53, 2012 (1984).

[31] A. Sandoval et al., Proceedings of the 7th High Energy Heavy Ion Study, Darmstadt, Germany, GSI Report GSI-85-10, 477 (1985).

[32] G. Odyniec et al., Proceedings of the 8th High Energy Heavy Ion Study, Berkeley, California, Lawrence Berkeley Laboratory Report LBL-24580, 215 (1988).

[33] S.I. Chase et al. Proceedings of the Workshop on Nuclear Dynamics VI, Jackson Hole, Wyoming, Lawrence Berkeley Laboratory Report LBL-28709, 67 (1990).

[34] This has also been observed in 1 GeV/n Ar + Ca $\rightarrow \pi^0$, see F.D. Berg et al., Z. Phys. A340, 297 (1991), and in Au + Au $\rightarrow \pi^0$, W. Kuehn and the TAPS Collaboration, GSI-Darmstadt Preprint (1992).

[35] E. Barasch et al., Phys. Lett. B161, 265 (1985).

[36] S. Schnetzer et al., Phys. Rev. Lett. 49, 989 (1982).

[37] It is important to note that this slope parameter was derived from an invariant distribution $E(d^3\sigma/dp^3)$, whereas only the momentum density distribution $d^3\sigma/dp^3$ should have exact exponential behavior.

[38] J. Sollfrank, P. Koch and U. Heinz, Phys. Lett. B252, 256 (1990).

[39] J.W. Harris et al., Nucl. Phys. A471, 241c (1987).

[40] K.G.R. Doss et al., Phys. Rev. Lett. 59, 2720 (1987).

[41] K.S. Lee and U. Heinz, Z. Phys. C43, 425 (1989).

[42] K.S. Lee, U. Heinz and E. Schnedermann, Z. Phys. C48, 525 (1990)

[43] J.W. Harris et al., Nucl. Phys. A498, 133c (1989).

[44] U. Heinz lectures in this School.

[45] NA5 Collaboration, private communication.

[46] W. Bell et al., Phys. Lett. B112, 271 (1982); A. Karabarbounis et al., Phys. Lett. B104, 75 (1981); A.L.S. Angelis et al., Phys. Lett. B116, 379 (1982).

[47] B. Jacak, Nucl. Phys. A525, 77c (1991).

[48] T. Matsui and H. Satz, Phys. Lett. 178B, 416 (1986).

[49] For details see lectures of G. Young in this School.

[50] H. Barz, G. Bertsch, B.L. Friman, H. Schulz and S. Boggs, Phys. Lett. 265B, 219 (1991).

[51] D. Lissauer and E.V. Shuryak, Phys. Lett. B253, 15 (1991).

[52] G.F. Bertsch, G.E. Brown, P. Koch and B.A. Li, Nucl. Phys. A490, 745 (1988).

[53] C. Gale and J. Kapusta, Phys. Rev. C35, 2107 (1987); C40, 2397 (9189).

[54] L.H. Xia, C.M. Ko, L. Xiong and J.Q. Wu, Nucl. Phys. A485, 721 (1988).

[55] C.M. Ko, L.H. Xia and P.J. Siemens, Phys. Lett. B231, 16 (1989).

[56] S. Mikamo et al., Phys. Lett. 106B, 428 (1981).

[57] J. Ballam et al., Phys. Rev. Lett. 41, 1207 (1978); D. Blockus et al., Nucl. Phys. B201, 205 (1982); and M.R. Adams et al., Phys. Rev. D27, 1977 (1983).

[58] A. Browman et al., Phys. Rev. Lett. 37, 246 (1976).

[59] G. Roche et al., Phys. Rev. Lett. 61, 1069 (1988).

[60] C. Naudet et al., Phys. Rev. Lett. 62, 2652 (1989).

[61] G. Roche et al., Phys. Rev. Lett. 61, 1069 (1988).

[62] G. Wolf et al., Nucl. Phys. A517, 615 (1990).

[63] L. Xiong et al., Phys. Rev. C41, R1355 (1990).

[64] H. Huang et al., submitted to Phys. Lett. B (1992).

[65] See proceedings of the 8th High Energy Heavy Ion Study, Lawrence Berkeley Laboratory Report LBL-24580 (1988), and references therein.

[66] S. Nagamiya, Nucl. Phys. A544, 5c (1992).

[67] T. Abbott et al., E802 Collaboration private communication (1992).

[68] S. Wenig (NA35 Collaboration), Ph.D. thesis, University of Frankfurt, GSI Report 90-23 (1990).

[69] L. Teitelbaum (NA35 Collaboration), Ph.D. thesis, University of California - Berkeley, Lawrence Berkeley Laboratory Report LBL-32812 (1992).

[70] K. Werner, Brookhaven National Laboratory Preprint BNL-42 435 (1989).
[71] H. Sorge et al., Ann. Phys. 192, 266 (1989).
[72] Th. Schoenfeld et al., Nucl. Phys. A544, 439c (1992) and references therein.
[73] R. Albrecht et al., Phys. Lett. B202, 596 (1988).
[74] L.M. Barbier et al., Phys. Rev. Lett. 60, 405 (1988).
[75] H. von Gersdorf et al., Phys. Rev. C39, 1385 (1989).
[76] L.D. Landau, Collected Papers, No. 88, Izv. Akad. Nauk, Ser. Fiz. 17, 51 (1953).
[77] B. Andersson et al., Nucl. Phys. B281, 289 (1987); B. Nilsson-Almqvist and E. Stenlund, Comp. Phys. Commun. 43, 387 (1987).
[78] See for example M. Prakash, Proceedings of the Workshop on Heavy Ion Physics at the AGS, Brookhaven National Laboratory Report BNL-44911, 371 (1990).
[79] J. Stachel and P. Braun-Munzinger, Phys. Lett. B216, 1 (1989).
[80] J. Kapusta, Nucl. Phys. 61, 461 (1980).
[81] J. Kuti et al., Phys. Lett. 95B, 75 (1980).
[82] H. Satz, Ann. Rev. Nucl. Part. Sci. 35, 245 (1985).
[83] Conceptual Design of the Relativistic Heavy Ion Collider, Brookhaven National Laboratory Report BNL-52195 (1989).
[84] For details see lecture of S. Ozaki in this School.
[85] Proposal on Spin Physics Using the RHIC Polarized Collider, RHIC Spin Collaboration (1992).
[86] F. Videbaek and T. Throwe, Fourth Workshop on Experiments and Detectors for a Relativistic Heavy Ion Collider, Brookhaven National Laboratory Report BNL-52262 (1990).
[87] STAR is the experiment further along in design and with which the author is most familiar.
[88] RHIC Letter of Intent for a Forward and a Midrapidity Hadron Spectrometer at RHIC, D. Beavis et al., Brookhaven National Laboratory Preprint (1990); Addendum (1991).
[89] RHIC Letter of Intent to Study Very Low p_t Phenomena at RHIC, PHOBOS Collaboration (1991).
[90] See lecture of W. Busza in this School.
[91] PHENIX Experiment at RHIC - Preliminary Conceptual Design Report, PHENIX Collaboration Report (1992).
[92] RHIC Letter of Intent for an Experiment on Particle and Jet Production at Midrapidity, The STAR Collaboration, Lawrence Berkeley Laboratory Report LBL-29651 (1990).
[93] Update to the RHIC Letter of Intent for an Experiment on Particle and Jet Production at Midrapidity, The STAR Collaboration, Lawrence Berkeley Laboratory Report LBL-31040 (1991).
[94] Conceptual Design Report for the Solenoidal Tracker At RHIC, The STAR Collaboration, PUB-5347 (1992).
[95] E.V. Shuryak and O.V. Zhirov, Phys. Lett. B89, 253 (1980); E.V. Shuryak and O.V. Zhirov, Phys. Lett. B171, 99 (1986).
[96] P.V. Ruuskanen, Z. Phys. C38, 219 (1988).
[97] K. Redlich and H. Satz, Phys. Rev. D33, 3747 (1986).
[98] P.V. Landshoff, Nucl. Phys. A498, 217 (1989).
[99] X.N. Wang, Lawrence Berkeley Laboratory Report LBL-28790 (1990).
[100] R. Anishetty, P. Koehler and L. McLerran, Phys. Rev. D22, 2793 (1980); W. Busza and A.S. Goldhaber, Phys. Lett. 139B, 235 (1984); S. Date, M. Gyulassy and H. Sumiyoshi, Phys. Rev. D32, 619 (1985).
[101] R. Hagedorn and J. Rafelski, Phys. Lett. 97B, 180 (1980); J. Rafelski and B. Mueller, Phys. Rev. Lett. 48, 1066 (1982); P. Koch, B. Mueller and J. Rafelski, Phys. Rep. 142, 167 (1986).
[102] N.K. Glendenning and J. Rafelski, Phys. Rev. C31, 823 (1985); K.S. Lee, M.J. Rhoades-Brown and U. Heinz, Phys. Rev. C37, 1452 (1988).
[103] J. Rafelski and A. Schnabel, "Intersections Between Nuclear and Particle Physics," AIP Proceedings No. 176, 1068 (1988), and references therein.
[104] J. Rafelski, Phys. Rep. 88, 331 (1982).
[105] A. Shor, Phys. Rev. Lett. 54, 1122 (1985).
[106] R. D. Pisarski and F. Wilczek, Phys. Rev. D29, 338 (1984).

[107] T. Hatsuda and T. Kunihiro, Phys. Lett. B185, 304 (1987).
[108] E.V. Shuryak, Nucl. Phys. A525, 3c (1991).
[109] C.E. DeTar and J.B. Kogut, Phys. Rev. Lett. 59, 399 (1987); Phys. Rev. D36, 2828 (1987).
[110] E.V.E. Kovacs et al., Phys. Rev. Lett. 58, 751 (1987); F. Karsch et al., Phys. Lett. 188B, 353 (1987).
[111] F.B. Yano and S.E. Koonin, Phys. Lett. B78, 556 (1978); K. Kolehmainen and M. Gyulassy, Phys. Lett. B180, 203 (1986); B. Andersson and W. Hofmann, Phys. Lett. B169, 364 (1986).
[112] A. Bamberger et al., Phys. Lett. B203, 320 (1988).
[113] S. Pratt, Phys. Rev. D33, 1314 (1986); G. Bertsch, M. Gong and M. Tohyama, Phys. Rev. C37, 1896 (1988) and G. Bertsch MSU Preprint (1988).
[114] P. Seyboth et al., Nucl. Phys. A544, 293c (1992).
[115] M. Gyulassy and S. S. Padula, Lawrence Berkeley Laboratory Report LBL-26077 (1988).
[116] K.S Lee, M.J. Rhoades-Brown and U. Heinz, Phys. Rev. C37, 1463 (1988).
[117] J.D. Bjorken and L.D. McLerran, Phys. Rev. D 20, 2353 (1979) and Y. Takahashi and S. Dake, Nucl. Phys. A461, 263C (1987).
[118] P.V. Ruuskanen, International Workshop on Quark-Gluon Plasma Signatures, Strasbourg, France, JYFL-3-90 Preprint (1990).
[119] M. Gyulassy, Nucl. Phys. A400, 31c (1983); L. Van Hove, Z. Phys. C27, 135 (1985).
[120] X.N. Wang and M. Gyulassy in Proceedings of the Workshop on Experiments and Detectors for RHIC, Brookhaven National Laboratory, Upton, New York, 2-7 July 1990, Brookhaven National Laboratory Report BNL-52262, 79 (1990) and references therein.
[121] K. Kajantie, P.V. Landshoff and J. Lindfors, Phys. Rev. Lett. 59, 2527 (1987).
[122] K.J. Eskola, K. Kajantie and J. Lindfors, Nucl. Phys. B323, 37 (1989).
[123] X.N. Wang, Lawrence Berkeley Laboratory Report LBL-28789 (1990).
[124] X.N. Wang and M. Gyulassy, Phys. Rev. Lett. 68, 1480 (1992).

LAWRENCE BERKELEY LABORATORY
UNIVERSITY OF CALIFORNIA
TECHNICAL INFORMATION DEPARTMENT
BERKELEY, CALIFORNIA 94720

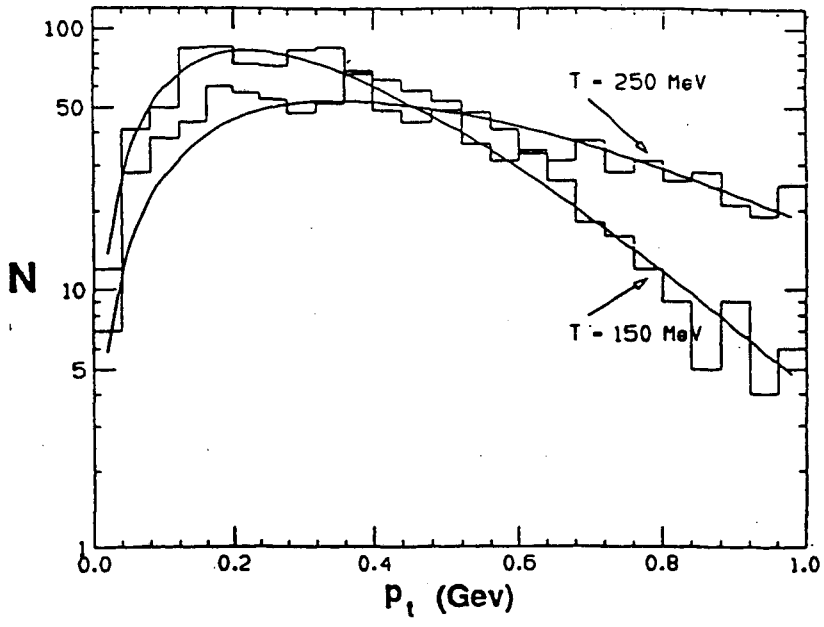

Figure 7. Simulation of the p_t spectrum for one event generated using a Boltzmann distribution of 1000 pions. The histograms correspond to single events generated with T = 150 MeV and 250 MeV. The curves are fits to the histogram using a Maxwell-Boltzmann distribution.

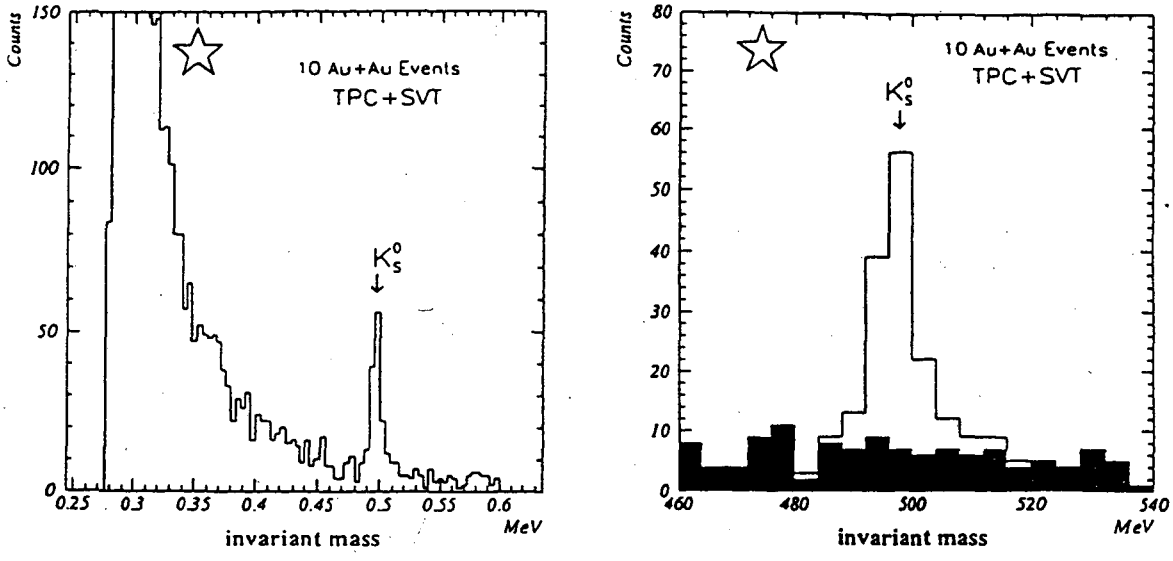

Figure 8. Simulated invariant mass distribution for $K^0_S \rightarrow \pi^+\pi^-$ measured in STAR for 10 central Au + Au events at RHIC. The right-hand side is an expanded view in the region of the K^0_S mass. The shaded area represents the contribution from random combinatorial background.

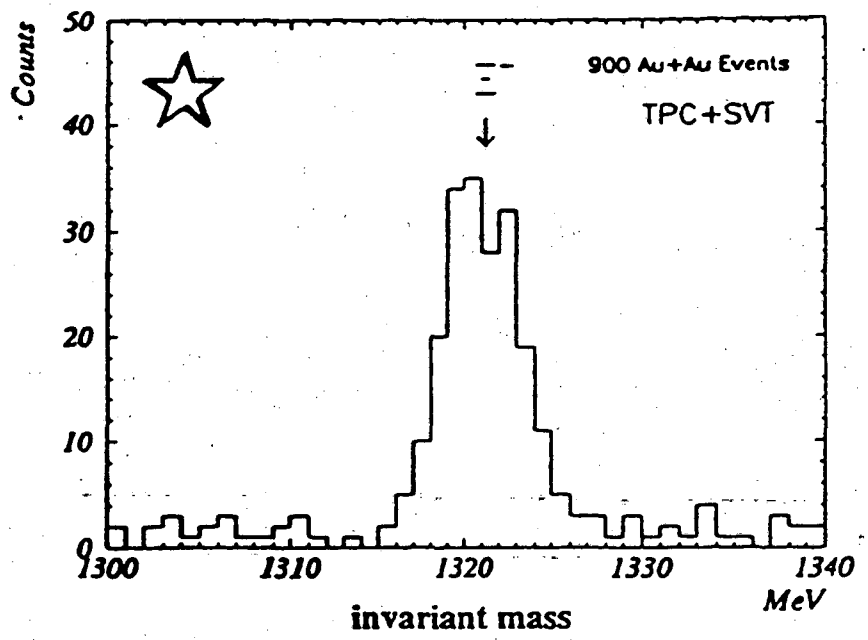

Figure 9. Simulated invariant mass distribution from the decay $\Xi^- \rightarrow \Lambda\pi^-$ with $\Lambda \rightarrow \pi^- p$ measured in STAR for 900 central Au + Au events at RHIC.

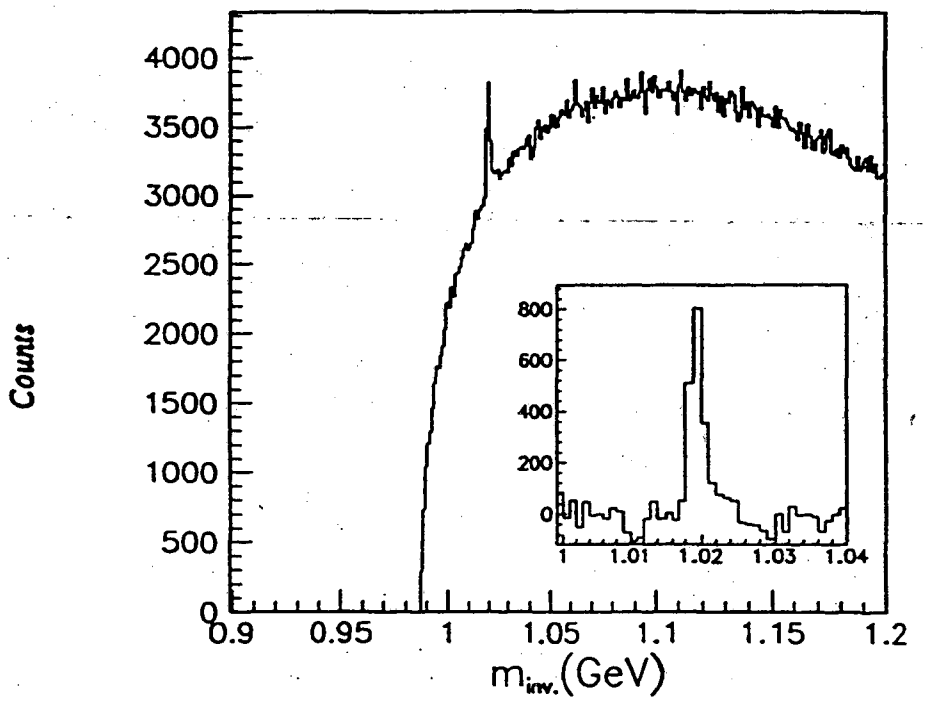

Figure 10. Invariant mass distribution for all identifiable K^+K^- pair combinations simulated in the acceptance $|\eta| < 1$ of STAR for 500 Au + Au central events at RHIC. The ϕ signal is the narrow peak at 1.02 GeV. The inset is the result of a subtraction of K^+K^- pairs formed from K^+ and K^-, each from a different event, from the true K^+K^- pairs of the main part of this figure. The simulation has no width for the ϕ and the contribution of the detector to the measurement of the ϕ is observed to be minimal compared to the true width of $\Gamma = 4.4$ MeV.

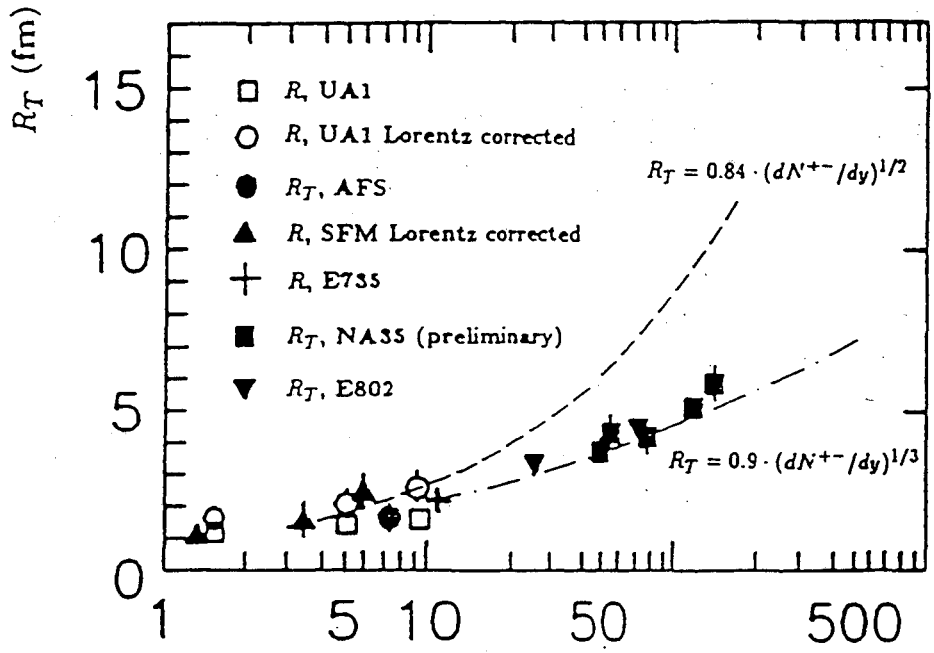

Figure 11. The correlation between the transverse source radii, derived from two-pion correlation measurements, and the charged-particle rapidity density at midrapidity. Measurements from the Sp $\bar{p}$S collider, ISR collider, Tevatron collider, Brookhaven AGS heavy ions and the CERN SPS heavy ions are presented. Two parameterizations corresponding to $R_t \sim (dn/dy)^{-1/2}$ and $R_t \sim (dn/dy)^{-1/3}$ are shown.

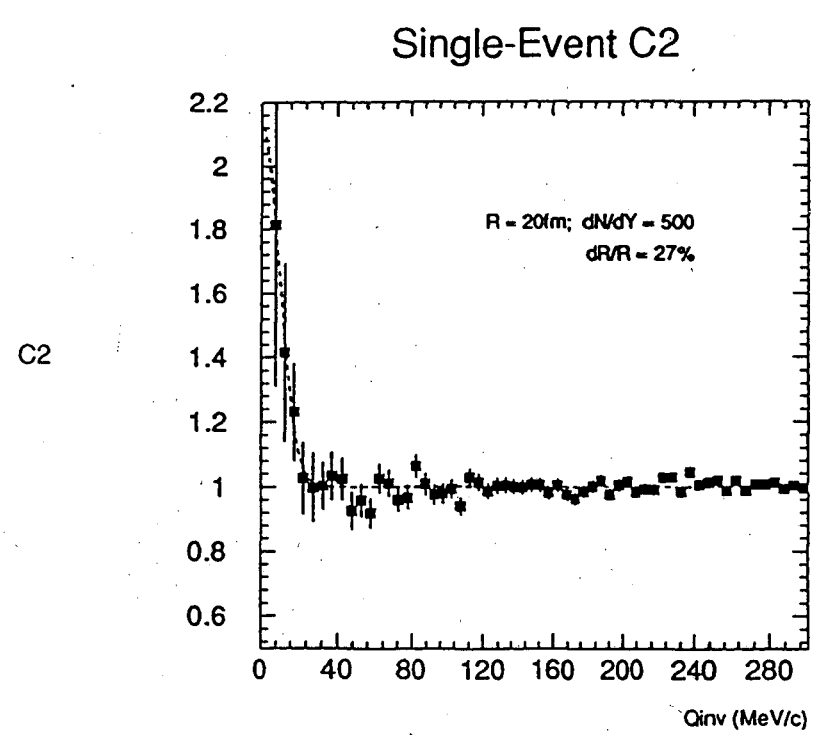

Figure 12. Correlation measurement for a single event simulated with $R_{inv} = 20$ fm and $dN_{\pi^-}/d\eta = 500$ in STAR at midrapidity.

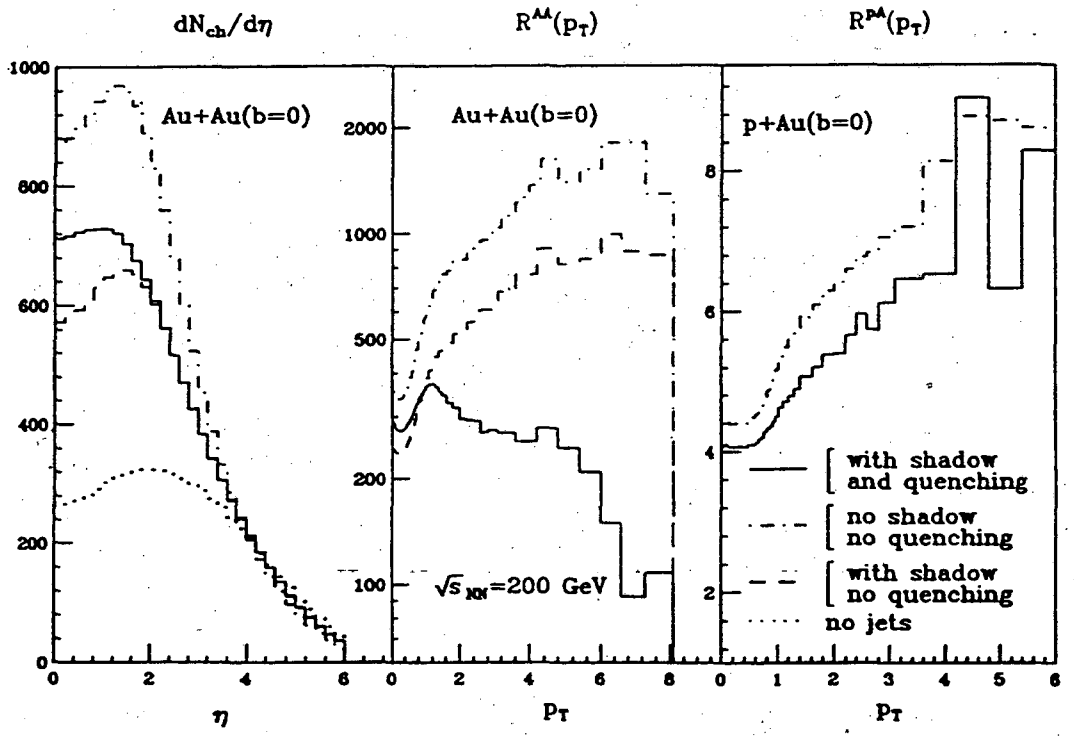

Figure 13. Results from HIJING calculations on the dependence of the inclusive charged hadron spectra in central Au + Au and p + Au collisions on minijet production (dash-dotted), gluon shadowing (dashed) and jet quenching (solid) assuming that the gluon shadowing is identical to that of quarks (see Ref. 56 for details). R^{AB} (p_t) is the ratio of the inclusive p_t spectrum of charged hadrons in A + B collisions to that of p + p.

LAWRENCE BERKELEY LABORATORY
UNIVERSITY OF CALIFORNIA
TECHNICAL INFORMATION DEPARTMENT
BERKELEY, CALIFORNIA 94720